

NAVAL POSTGRADUATE SCHOOL

Monterey, California



THESIS

**SUPPRESSION OF MARINE STRATOCUMULUS CLOUDS
DUE TO REDUCED CLOUD CONDENSATION NUCLEI**

by

Neil Tyler Smith

September 2000

Thesis Advisor:
Second Reader:

Philip A. Durkee
Qing Wang

Approved for public release, distribution is unlimited.

20001205 018

REPORT DOCUMENTATION PAGE			Form Approved OMB No. 0704-0188	
Public reporting burden for this collection of information is estimated to average 1 hour per response, including the time for reviewing instruction, searching existing data sources, gathering and maintaining the data needed, and completing and reviewing the collection of information. Send comments regarding this burden estimate or any other aspect of this collection of information, including suggestions for reducing this burden, to Washington headquarters Services, Directorate for Information Operations and Reports, 1215 Jefferson Davis Highway, Suite 1204, Arlington, VA 22202-4302, and to the Office of Management and Budget, Paperwork Reduction Project (0704-0188) Washington DC 20503.				
1. AGENCY USE ONLY (Leave blank)		2. REPORT DATE September 2000		3. REPORT TYPE AND DATES COVERED Master's Thesis
TITLE AND SUBTITLE : Suppression of Marine Stratocumulus Clouds Due to Reduced Cloud Condensation Nuclei			5. FUNDING NUMBERS	
6. AUTHOR(S) Neil Tyler Smith				
7. PERFORMING ORGANIZATION NAME(S) AND ADDRESS(ES) Naval Postgraduate School Monterey, CA 93943-5000			8. PERFORMING ORGANIZATION REPORT NUMBER	
9. SPONSORING / MONITORING AGENCY NAME(S) AND ADDRESS(ES) N/A			10. SPONSORING / MONITORING AGENCY REPORT NUMBER	
11. SUPPLEMENTARY NOTES The views expressed in this thesis are those of the author and do not reflect the official policy or position of the Department of Defense or the U.S. Government.				
12a. DISTRIBUTION / AVAILABILITY STATEMENT Approved for public release, distribution is unlimited.			12b. DISTRIBUTION CODE	
<p>ABSTRACT (maximum 200 words) Cloud researchers have documented a variety of processes at work in the formation and dissipation of clouds in the marine boundary layer (MBL). Cloud rifts occasionally mark a distinct exception to the continuity and broad coverage more commonly observed with these clouds. A possible explanation for the presence of large features of broken cloudiness embedded in stratocumulus is the removal of CCN by nucleation scavenging and drizzle.</p> <p>A cloud rift feature embedded in marine stratocumulus was observed in satellite imagery on July 16, 1999. A CIRPAS Twin Otter aircraft flew repeated crossings of the rift boundary while completing a comprehensive survey of the area. A comparison of microphysics and thermodynamics on opposite sides of the rift boundary indicate that these rifts form where low aerosol concentrations enhance drizzle production. Marine boundary layer aerosol concentrations in the rift were only 1/6 that observed below the background stratocumulus. Cloud droplets in rift clouds were 3-5 microns larger than droplets in stratocumulus and exhibited a broader size distribution. Drizzle observations were strongly correlated with the rift and calculations support a drizzle hypothesis for rift formation and maintenance. Aerosol losses can be accounted for in drizzle droplets and the disruption of the cloud layer evolves in a manner described by Ackerman (1993).</p>				
14. SUBJECT TERMS Marine Clouds, Precipitation, Aerosol, Marine Atmospheric Boundary Layer			15. NUMBER OF PAGES 72	
			16. PRICE CODE	
17. SECURITY CLASSIFICATION OF REPORT Unclassified	18. SECURITY CLASSIFICATION OF THIS PAGE Unclassified	19. SECURITY CLASSIFICATION OF ABSTRACT Unclassified	20. LIMITATION OF ABSTRACT UL	

THIS PAGE INTENTIONALLY LEFT BLANK

Approved for public release, distribution is unlimited.

**SUPPRESSION OF MARINE STRATOCUMULUS CLOUDS DUE TO
REDUCED CLOUD CONDENSATION NUCLEI**

Neil Tyler Smith
Lieutenant, United States Navy
B.S., Texas A&M University, 1994

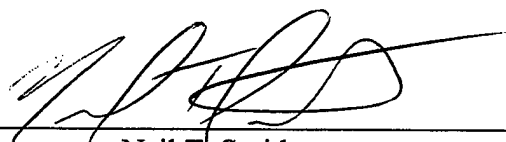
Submitted in partial fulfillment of the
requirements for the degree of

MASTER OF SCIENCE IN METEOROLOGY AND PHYSICAL OCEANOGRAPHY


from the


**NAVAL POSTGRADUATE SCHOOL
September 2000**


Author:


Neil T. Smith

Approved by:


Philip A. Durkee, Thesis Advisor


For Qing Wang, Second Reader


For Dr. Carlyle H. Wash, Chairman
Department of Meteorology

THIS PAGE INTENTIONALLY LEFT BLANK

ABSTRACT

Cloud researchers have documented a variety of processes at work in the formation and dissipation of clouds in the marine boundary layer (MBL). Cloud rifts occasionally mark a distinct exception to the continuity and broad coverage more commonly observed with these clouds. A possible explanation for the presence of large features of broken cloudiness embedded in stratocumulus is the removal of CCN by nucleation scavenging and drizzle.

A cloud rift feature embedded in marine stratocumulus was observed in satellite imagery on July 16, 1999. A CIRPAS Twin Otter aircraft flew repeated crossings of the rift boundary while completing a comprehensive survey of the area. A comparison of microphysics and thermodynamics on opposite sides of the rift boundary indicate that these rifts form where low aerosol concentrations enhance drizzle production. Marine boundary layer aerosol concentrations in the rift were only 1/6 that observed below the background stratocumulus. Cloud droplets in rift clouds were 3-5 microns larger than droplets in stratocumulus and exhibited a broader size distribution. Drizzle observations were strongly correlated with the rift and calculations support a drizzle hypothesis for rift formation and maintenance. Aerosol losses can be accounted for in drizzle droplets and the disruption of the cloud layer evolves in a manner described by Ackerman (1993).

THIS PAGE INTENTIONALLY LEFT BLANK

TABLE OF CONTENTS

I.	INTRODUCTION.....	1
A.	BACKGROUND	1
B.	MOTIVATION	1
II.	THEORY	5
A.	MARINE CLOUD CHARACTERISTICS.....	5
1.	Drizzle Production in Marine Stratocumulus.....	6
2.	Aerosols and Cloud Microphysics	7
B.	CLOUD LIFE CYCLE THEORIES	9
1.	Cloud Top Entrainment Instability	10
2.	Scavenging of Hygroscopic Nuclei in Marine Clouds	10
a.	Cloud Optical Thickness.....	11
b.	Cloud Condensation Nuclei Scavenging	11
III.	DATA COLLECTION AND ANALYSIS	13
A.	EXPERIMENTAL SETUP	13
1.	Synoptic Conditions.....	13
2.	Rift Evolution	14
3.	Data Collection.....	15
a.	Thermodynamics.....	15
b.	Cloud Microphysics	16
B.	ANALYSIS PROCEDURE	19
1.	Background Clouds, Station Sierra	20
2.	Rift clouds, Station Tango.....	20
3.	Cloud Rift Edge.....	20
C.	DATA AND ANALYSIS	21
1.	Description of the Background Cloud, Station Sierra	21
2.	Description of the Rift Area, Station Tango.....	22
3.	Description of the Rift Edge.....	24
4.	Rift Drizzle	26
5.	Cloud-topped Boundary Layer	28
IV.	CONCLUSION	41
A.	FINDINGS	41
B.	RECOMMENDATIONS.....	42
	LIST OF REFERENCES	43
	APPENDIX.....	45
	INITIAL DISTRIBUTION LIST	53

THIS PAGE INTENTIONALLY LEFT BLANK

LIST OF FIGURES

Figure 1. Cloud Rifts.	3
Figure 2. Cloud Droplet Population Comparison.	6
Figure 3. Evolution of Simulated Cloud Properties.	12
Figure 4. Stations Sierra and Tango.	17
Figure 5. Surface Pressure.	18
Figure 6. Evolution of the Cloud Rift.	18
Figure 7. Flight Track Schematic.	21
Figure 8. Boundary Layer Thermodynamics.	29
Figure 9. Liquid Water Concentration.	30
Figure 10. Cloud Droplets in Vertical Soundings.	31
Figure 11. Aerosol in Vertical Soundings.	32
Figure 12. Rift Crossing at 30 m.	33
Figure 13. Rift Crossing at 200 m.	34
Figure 14. Rift Crossing at 630 m.	35
Figure 15. Drizzle Frequency.	36
Figure 16. Drizzle Model.	37
Figure 17. Cloud Top Flight Track.	37
Figure 18. Rift Crossing at Cloud Tops.	38
Figure 19. Rift Microphysics.	39

THIS PAGE INTENTIONALLY LEFT BLANK

LIST OF TABLES

Table 1. Flight Path Summary	19
Table 2. Liquid Water Calculations	27

THIS PAGE INTENTIONALLY LEFT BLANK

ACKNOWLEDGMENTS

Nurturing a student tackling a project of this scope requires a great amount of patience and guidance. Professor Philip Durkee epitomized these qualities all the way through. He deserves most of the credit for getting this project safely home. Hafliði Jonsson delivered an essential element of this thesis, the in-situ data collected by the CIRPAS Twin Otter aircraft. Haf labored for months preparing for the mission, collecting and processing the data, and ultimately getting it to us for analysis. Thank you, Haf. I hope this thesis faithfully delivers a fraction of the information you skillfully exacted from virtually thin air.

Additional motivation and a proper perspective was infused from many sources. I work among terrific officers who exemplify sacrifice and commitment while retaining a great sense of what's important outside of academics. Friends at the Monterey Bay Aquarium provided much needed support and endless opportunities for social gathering. Other faculty in the department were inspirations as well. Professor Ken Davidson and I share a love for running, and he took the time to keep up on my training regimen. My training regimen has fallen apart in the past few months if you must know professor. And Kurt Nielson lent an expert's hand down in the Remote Sensing Lab. A final debt of gratitude is felt for my girlfriend, Megan Lewis. She lifts my spirits and inspires me to action just by loving me. Her smile alone brightens a full day, and that's something this seaside villager needed occasionally.

THIS PAGE INTENTIONALLY LEFT BLANK

I. INTRODUCTION

A. BACKGROUND

Marine stratocumulus clouds are a persistent and important feature of the marine boundary layer normally found on eastern ocean basins. Persistent marine stratocumulus develop more frequently in summer, when the subtropical high has moved northward and strong subsidence occurs along its eastern edge. Along the west coast of North America, cool upwelled water contributes to boundary layer inversion strength, fostering cloud formation and persistence. Generally, the inversion slopes upward from east to west along a line stretching from California to Hawaii and stratocumulus clouds drifting along a southwesterly track break up into cumulus fields as a result of weakening large-scale subsidence and increasing sea surface temperature.

Researchers have been studying processes associated with marine stratocumulus cloud formation, persistence, and dissipation. This research has produced a large body of science describing general marine boundary layer cloud characteristics. Previous research has capitalized on special circumstances in the atmosphere that provide field data to test theories. One example is a ship track. Ship tracks offer evidence to support cloud reflectivity and stability theories (Durkee et al. 2000). Overall, the discoveries reveal interactions that are both complex and subtle, posing deeper questions concerning the cycle of stratocumulus formation and dissipation.

B. MOTIVATION

Marine stratocumulus clouds blanket hundreds of thousands of square kilometers of ocean. International efforts to quantify the significance of marine clouds have revealed

that stratiform clouds overlie a third of the ocean surface (Warren et al., 1988). The low-level clouds have warm cloud tops emitting infrared back into space and are highly reflective returning shortwave solar as well. The net effect of low clouds over the ocean is to cool the Earth. Research clearly supports the importance of low clouds to the overall radiation heat budget. Randall and Coakley (1984) demonstrated in a model that a mere 4% increase in low cloud fractional coverage would compensate for the doubling of CO₂, a greenhouse gas implicated in global warming.

The variability of marine stratocumulus clouds under the subtropical high is a key factor in the net cooling effect generated by maritime clouds. Several experiments have demonstrated that aerosols, including anthropogenic aerosols, modify marine cloud persistence and reflectivity. Phenomena like ship tracks are dramatic examples of anthropogenic forcing of cloud reflectivity and persistence. Cloud rifts are another phenomena often present in marine stratocumulus. 'Cloud rift' describes an element of broken clouds embedded in the background stratocumulus field. Rifts are distinct features in visible satellite imagery due to low pixel brightness values. Hindman et al. (1994) describes a broken cloud feature in its study of ship tracks. The air mass is near saturation, unstable, drizzling and characterized by a small number of aerosols. The cloud rifts observed on July 16th, 1999 are shown in Figure 1. Rifts are seen stretching well offshore and have opened a large fraction of the background stratocumulus. Ship tracks persisted inside the rift and are the thin linear clouds running to the northwest. The three largest rift features cleared approximately 200,000 km².

The objective of this study is to investigate possible factors contributing to cloud rifts and the suppression of the marine stratocumulus deck. Investigating the lifecycle of cloud rifts with a variety of sensors to include satellite, atmospheric models, and research aircraft may provide insights into key processes linked to stratocumulus growth and dissipation. Cloud rifts are in effect naturally occurring laboratories useful to researchers studying the marine boundary layer. Judging from the character of the cloud rifts and based upon cloud dissipation theories presented in the next chapter, cloud rifts are most likely the result of nucleation scavenging of cloud condensation aerosols and marine cloud drizzle.

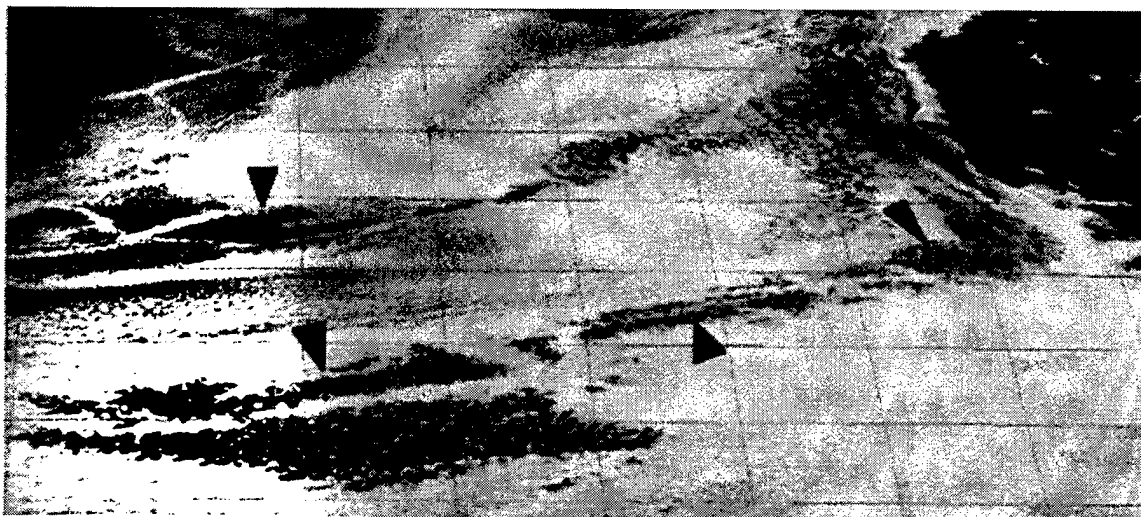


Figure 1. Cloud Rifts. Markers indicate locations of rifts embedded in the background stratocumulus. This visible satellite image was taken on July 16, 1999 at 1600 UTC.

THIS PAGE INTENTIONALLY LEFT BLANK

II. THEORY

A. MARINE CLOUD CHARACTERISTICS

A cloud is described as an assembly of tiny droplets usually numbering several hundred per cubic centimeter with an average size of about ten microns. Droplets in a cloud are referred to as populations, and the population is normally stable – changing primarily due to variations in supersaturation. Marine clouds share many common features with continental clouds, but do have distinct cloud droplet populations. Figure 2 depicts this difference in size distribution and concentration. Marine clouds are characterized by fewer cloud droplets in a broader and larger size distribution than continental clouds. In stable clouds, droplet populations grow together as supersaturation controls condensational growth. Collision and coalescence of droplets is not appreciable in clouds containing small, narrow droplet distributions. However, marine clouds often have wide distributions of sizes and the differential fall velocities of different drop sizes increase collisions and the formation of large droplets. Once a threshold of disparity in droplet size is reached, collision and coalescence will destabilize the cloud drop population, rapidly generate large drops, and lead to light precipitation often referred to as drizzle.

Studies of broken clouds over the Pacific Ocean show that relatively aerosol free regions remain cloud free while producing drizzle conditions in nearly saturated air masses (Hindman et al. 1994, Ferek et al. 2000). A possible explanation is that very low aerosol densities enhance drizzle production breaking up marine stratocumulus. Marine cloud studies by Albrecht (1989), Hudson and Frisbie (1991) and Hindman et al. (1994) observe

aerosol losses and cloud microphysics that support a dissipation mechanism marked by drizzle.

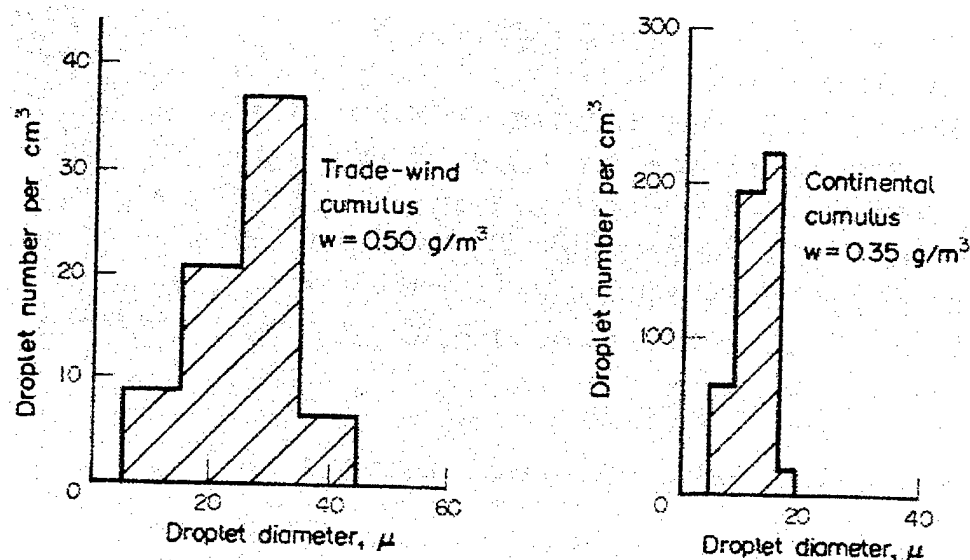


Figure 2. Cloud Droplet Population Comparison. From Rogers and Yau (1989).

1. Drizzle Production in Marine Stratocumulus

An understanding of the drizzle process is necessary to properly describe the cloud rift process. Drizzle is often observed in marine stratocumulus clouds. Drizzle describes cloud droplets on the verge of becoming rain drops. Rain drops are defined as drops large enough to reach the ground before evaporating. Rain drops are typically on the order of one to two millimeters radius, but drops larger than 0.1 mm radius often reach the ground before evaporating. Rain drops smaller than 0.1 mm are designated as drizzle (Rogers, 1989).

Drizzle is a warm cloud process in the marine boundary. Clouds with populations averaging 10 microns are generally stable and cloud droplet populations will grow uniformly. Precipitation occurs when the cloud droplets become so large that collisions

occur frequently producing even larger droplets. Cloud droplet populations experience asymmetric growth leading to precipitation if either of two events occur (Rogers, 1989):

1. Radial sizes exceed $20\text{ }\mu\text{m}$
2. Ice crystals form

Thermodynamic conditions in the coastal marine boundary layer are not favorable for ice crystal formation, but the growth of droplets to instability thresholds is likely, especially when cloud condensation nuclei levels are low.

2. Aerosols and Cloud Microphysics

Aerosol particles are an integral part of the lifecycle of marine clouds. Aerosols range in size from $0.001\text{ }\mu\text{m}$ to $10\text{ }\mu\text{m}$. Aerosols are concentrated in the troposphere and are subject to complex production and removal processes – much like the clouds they influence. Hygroscopic aerosols act as catalysts in cloud formation by reducing saturation requirements for cloud droplet production. Hygroscopic aerosols dissociate in a reaction with water and reduce the saturation vapor pressure necessary for condensation. Aerosols serving as condensation sites that become cloud droplets are designated cloud condensation nuclei (CCN). The identities and formation processes of these special hygroscopic nuclei are less understood and the subject of ongoing research. In general, cloud condensation nuclei comprise a fraction of the total aerosol population.

Twomey et al. (1984) discovered a property of cloud reflectivity that ties aerosol concentration to the radiative forcing of clouds. Specifically, cloud reflectivity is affected by CCN concentrations. A cloud with higher CCN concentrations is more reflective because the cloud droplet size distribution tends toward greater numbers of smaller cloud

droplets. Cloud optical thickness(δ) is determined by several microphysical properties of the cloud:

$$\delta = \frac{3wh}{2r_{eff}} \quad (1)$$

Optical thickness and cloud top brightness increase with water content, w , and cloud thickness, h , but decrease as effective droplet size increases.

Baker (1997) carries forward this important relationship between aerosols and clouds in a hypothesis linking marine stratocumulus to the global radiative budget. Cloud droplet size distributions in marine stratocumulus tend to be skewed toward fewer, larger drops than continental stratocumulus. The proportionate increase in reflectivity resulting from a given increase in aerosol concentration for marine clouds exceeds that for continental clouds, as indicated by the following equation.

$$\Delta\alpha \propto \frac{\Delta N}{N} \quad (2)$$

Here, α denotes cloud reflectivity, or albedo. Given the cooling properties associated with marine stratocumulus and the proximity to aerosol sources, these clouds may amplify the effects of tropospheric aerosol sources.

Many previous efforts focused on the interaction between clouds and aerosols. Albrecht (1989) evaluates data collected in the First ISCCP (International Satellite Cloud Climatology Program) Regional Experiment and finds the following:

1. Cloud condensation nuclei concentration, [CCN], increases result in higher cloud colloidal stability and increased cloud fractional coverage.
2. Clouds selectively remove soluble aerosol particles, clearly evident in shifts in CCN populations.

The data collected indicates that clouds are efficient sinks of aerosols, especially CCN. High aerosol concentrations are linked to cloud stability and greater cloud coverage.

Hudson and Frisbie (1991) use the same data set to investigate how stratocumulus clouds act as sinks for aerosol particles. The research observes the following process:

1. Nucleation scavenging as cloud droplets form.
2. Removal by precipitation or merely by the coalescence of individual cloud droplets.

Observations of aerosol concentrations in a cloud-topped boundary over a four day period showed reductions of approximately $50 \text{ particles cm}^{-3} \text{ day}^{-1}$. The research also notes the importance of aerosol sources in the maintenance of marine clouds.

B. CLOUD LIFE CYCLE THEORIES

Cloud development and dissipation in the marine environment has links to many atmospheric processes. In general, turbulence mixing within the cloudy boundary layer, generated mainly through infrared radiative cooling at the cloud top, is crucial in maintaining the cloud layer (e.g., Nicholls 1984). Several theories explain the dissipation of clouds in the marine boundary layer and are discussed in the following sub-sections.

1. Cloud Top Entrainment Instability

Cloud top entrainment instability theory was proposed by Randall (1980) as a model to describe cloud dissipation under strong subsidence conditions of subtropical highs. In order for evaporative cooling to proceed without creating instability within the cloud, the equivalent potential temperature(θ_e) must satisfy the relationship described in Eq.(3), which essentially states that the inversion above the cloud must not be too dry to have evaporative cooling in the entrainment mixing parcel dominate warming through direct mixing between the boundary layer air and the inversion air. Recent experiments by Kuo and Schubert (1988) tested the stability criteria. In defining the stability criterion for marine stratocumulus, a jump operator(Δ) is defined as the above-cloud value minus the in-cloud value. The parameters governing stability are gradients in θ_e and the total water mixing ratio(r).

$$\Delta\theta_e > k(L/c_p)\Delta r \quad (3)$$

L is the latent heat of condensation, c_p is the constant pressure heat capacitance, and k is a dimensionless constant of about 0.23. Using measurements from several field experiments, Kuo and Schubert (1988) suggested that dissatisfying Eq.(3) was insufficient to denote the onset of cloud breakup. Siems et al. (1990) proposes a corrected conditional test that is even more restrictive for marine cloud instability.

2. Scavenging of Hygroscopic Nuclei in Marine Clouds

Marine stratocumulus are influenced by various aerosol sources and sinks. Cloud scavenging and deposition of CCN remove aerosols while entrainment, sea spray or bubbles, and the condensation of marine gases supply the boundary layer with new

aerosols. Hudson and Frisbie (1991) observe that low aerosol concentrations above the inversion may disrupt the cloud stability. Cloud scavenging proceeds without sufficient resupply of aerosol, depleting CCN.

a. Cloud Optical Thickness

Drizzle is linked to cloud dissipation through a process described by Ackerman et al. (1993). In the Ackerman model, drizzle in marine stratocumulus reduces [CCN] and drives a change in cloud microphysics that eventually diminishes cloud top radiative cooling. Figure 3 shows the evolution of a marine cloud in a model simulation from Ackerman et al. (1993). In this simulation, drizzle begins at time zero and is sustained for three days while aerosol sources are turned off. Figures 3-A, 3-B and 3-C chronicle a decrease in cloud droplet concentration, increase in droplet size, and decrease in LWC associated with a shrinking CCN population. Figure 3-D shows that the cloud optical depth drops in response to the changing microphysics. The cooling profile, linked to cloud optical depth, descends into the cloud. Figure 3-E shows the evolution of cloud structure over the same time period. It appears from this experiment that drizzle can disrupt turbulence mixing in the marine boundary layer and eventually dissipate the cloud.

b. Cloud Condensation Nuclei Scavenging

The alternative process for cloud dissipation by depletion of CCN is the development of an evaporative inversion below the cloud deck. The Albrecht (1989) cloud model demonstrates that stratocumulus with low CCN concentrations have a higher precipitation efficiency and produce enhanced drizzle. The research indicates that drizzle production of 1 mm day^{-1} can deplete CCN concentrations by up to $1000\text{ cm}^{-3}\text{ day}^{-1}$. The boundary layer model also produces $10\text{ C km}^{-1}\text{ day}^{-1}$ cooling in a 500 m layer below the

cloud while some warming occurs in cloud due to latent heat release of condensation. This mechanism is proposed for the transition to trade cumulus on the southeast quadrant of the East Pacific high.

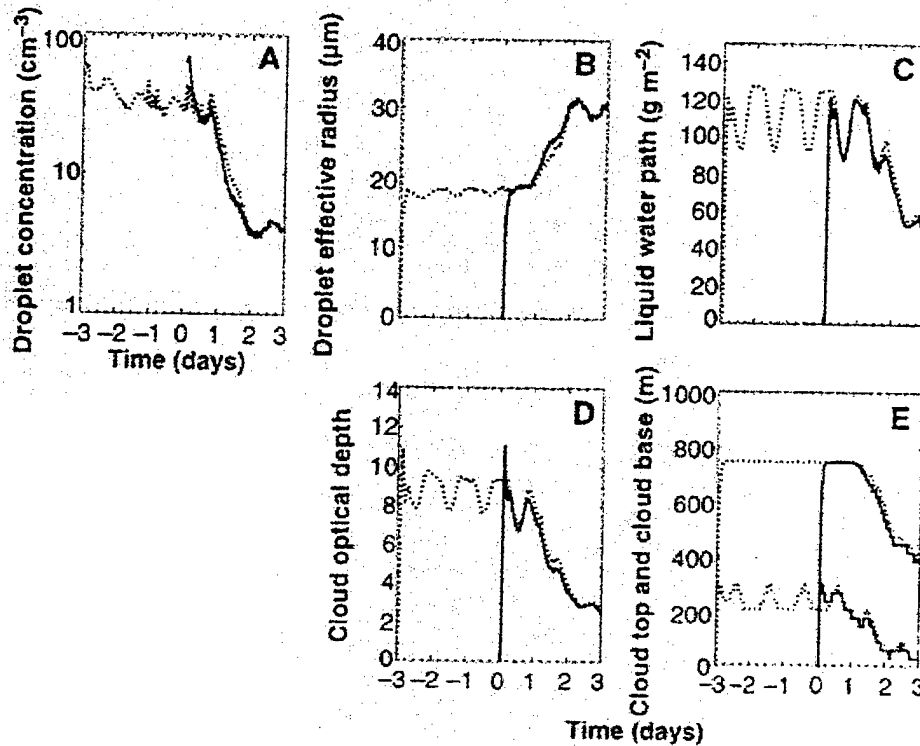


Figure 3. Evolution of Simulated Cloud Properties. 3-A depicts a drop in cloud droplet population associated with scavenging of cloud CCN without replenishment sources. 3-B depicts a rapid growth in effective radius. 3-C shows a diurnal feature in LWC but a decreasing trend. 3-D shows that reducing [CCN] reduces cloud optical depth. 3-E shows model cloud tops and bases lowering in response to microphysical forcing. From Ackerman et al. (1993).

III. DATA COLLECTION AND ANALYSIS

A. EXPERIMENTAL SETUP

A cloud rift feature was observed in satellite data on the morning of July 16, 1999. A Center for Interdisciplinary Remotely Piloted Aircraft Studies (CIRPAS) Twin Otter performed repeated crossings of the rift boundary to collect in-situ data at various altitudes. Sensors onboard the aircraft recorded data using a sampling rate of one hertz or higher. The data record lasts for more than three hours and surveys an area stretching approximately 400 kilometers. The rift boundary and related regions of interest to this study lie on a north-south track 70 kilometers in length. Two fixed stations shown in Figure 4-A and 4-B anchored the rift survey. Sierra was located at 36:42 N, 124:40 W and Tango at 36:08 N, 124:15 W for the first leg of the survey. Sierra marks the northernmost point along the track and remains within background stratocumulus for the entire field experiment. Tango marks the southernmost point and remained within the cloud rift region but did not remain cloud free for the entire survey. Section A in the Appendix contains additional details about the data collected, how it was used, and plan and profile views of the flight track.

1. Synoptic Conditions

Meteorological conditions for the period of July 15 and July 16, 1999 are typical of summer months along the California coast. A 1032 millibar high centered northwest of Monterey Bay provided subsidence conditions and northwesterly winds along the coast and far offshore. Upwelling of the coastal water and a persistent large-scale subsidence are elements fostering stratocumulus and both were present during the study. Figure 5

shows the surface pressure analysis for July 16, 1999. This chart is derived from model analysis fields archived at the Climatological Data Center in Asheville, N.C. Cloud drift winds analyzed for the survey period are geostrophic and indicate winds averaging 15 knots near the rift elements.

2. Rift Evolution

Satellite images taken by the GOES imager record the dynamic nature of cloud rifts. Two patches in the visible cloud imagery capture a glimpse of the cloud rift formation process. The satellite sequence in Figure 6 shows the rapid transition to rift cloudiness. The visible image in Figure 6-A taken at 0000 UTC on July 16th indicates some thinning of the stratocumulus layer in the marked regions. Figure 6-B shows the same cloud features 16 hours later. The imagery reveals that the clouds changed significantly by late morning July 16. Rifts occupy large areas once blanketed by clouds. Satellite analysis of the rift evolution that day reveal additional rift growth and cloud suppression. The rift size nearly doubles from 140,000 km² at 1500 UTC to just over 250,000 km² at 2100 UTC. The cloud rift perimeter appears to grow in an incremental fashion as cloud elements collapse near the rift edge. Cloud colloidal stability may be disrupted in clouds near the boundary, expanding the rift feature at the expense of background stratocumulus.

The rift elements are embedded in the background stratocumulus clouds for the entire period of observation. Rift motions match that of the surrounding stratocumulus clouds. The translation speed of the rift edge seen in Figure 4 over the three hour period of this study is roughly 14 knots. This is comparable to cloud drift wind measurements near the rift feature. The major rift axis is oriented perpendicular to apparent cloud motions. Satellite and geostrophic analysis indicate that the rifts are being advected with the air parcels.

3. Data Collection

The Twin Otter aircraft was equipped with over 30 sensors affixed on the wings, the nose and the fuselage. The array of sensors enabled an analysis of cloud thermodynamics and microphysics. A complete inventory of onboard sensors is listed in Table A-1 in the Appendix.

a. Thermodynamics

Thermodynamic properties associated with clouds are a useful tool to study air motions. Analysis of the cloud features began with temperature and dew point profiles at points of interest along the flight path. This information provides a measure of the inversion properties and the overall boundary layer vertical structure. Liquid water content (LWC) were measured using a Gerber PVM 100A sensor. The liquid water traces made for Sierra and Tango are useful in estimating cloud optical thickness and defining cloud levels in the flight record.

b. Cloud Microphysics

An array of particle sensors equipped the aircraft to study particle sizes ranging from fine aerosols to drizzle size cloud droplets. The different sensors provide coverage for a particular size range of atmospheric constituents. The Passive Cavity Aerosol Spectrometer Probe (PCASP) used in this survey is an aerosol particle measuring instrument. The Forward Scattering Spectrometer Probe (FSSP) measures particles in the range from 1 to 15 microns radius. This size range observes cloud droplets and is a useful instrument to study cloud droplet populations. The Cloud and Aerosol and Spectrometer (CAS) provides redundant coverage of the larger sizes measured by the PCASP sensor and all of the FSSP sensor but in a coarser fashion. A particular channel of the CAS (channel 14) is sensitive to particles ranging in radial size from 6 to 16 microns. Thus, channel fourteen covers nineteen distinct channels in the FSSP spectrum, and provides a cumulative check of the FSSP sensor. This survey was the first to use a new sensor to measure drizzle and precipitation. The Cloud Imaging Probe (CIP) provided data critical to evaluating the drizzle intensity associated with the rift. The CIP sensor is an occultation probe capable of measuring droplets ranging in size from 12.5 to 250 microns radius. Section B in the Appendix provides additional information about the probes and defines microphysical terms used to describe the rift event. The data collected by particle sensors on the Twin Otter was fairly clean and comparisons between sensors correlate very well.

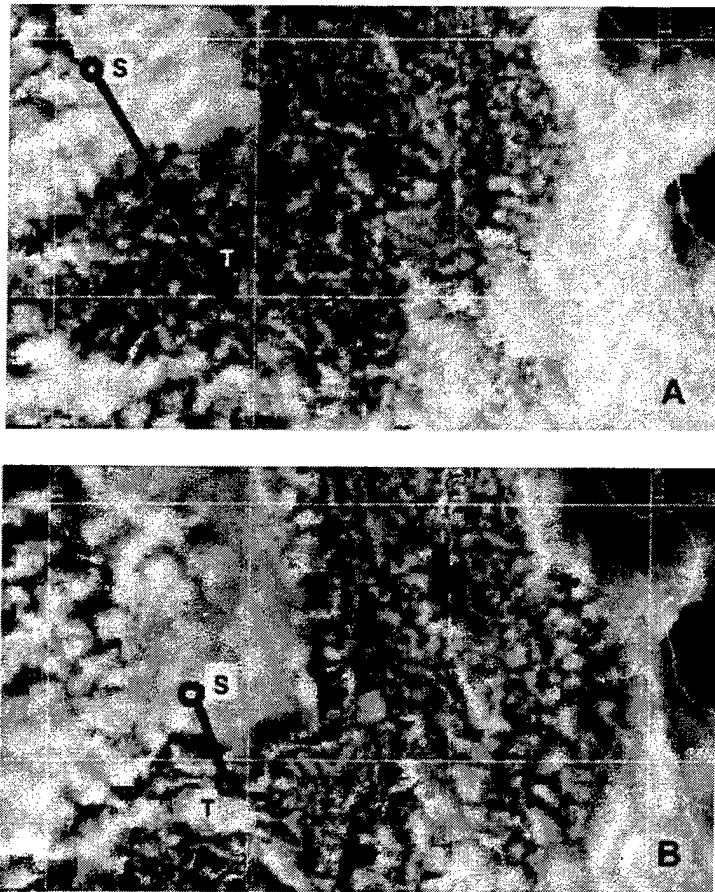


Figure 4. Stations Sierra and Tango. Survey areas moved during the experiment to capture cloud elements on both sides of the rift boundary. 4-A shows station positions early in the record, 1830 UTC. 4-B shows the flight track at the end of the mission, 2100 UTC.

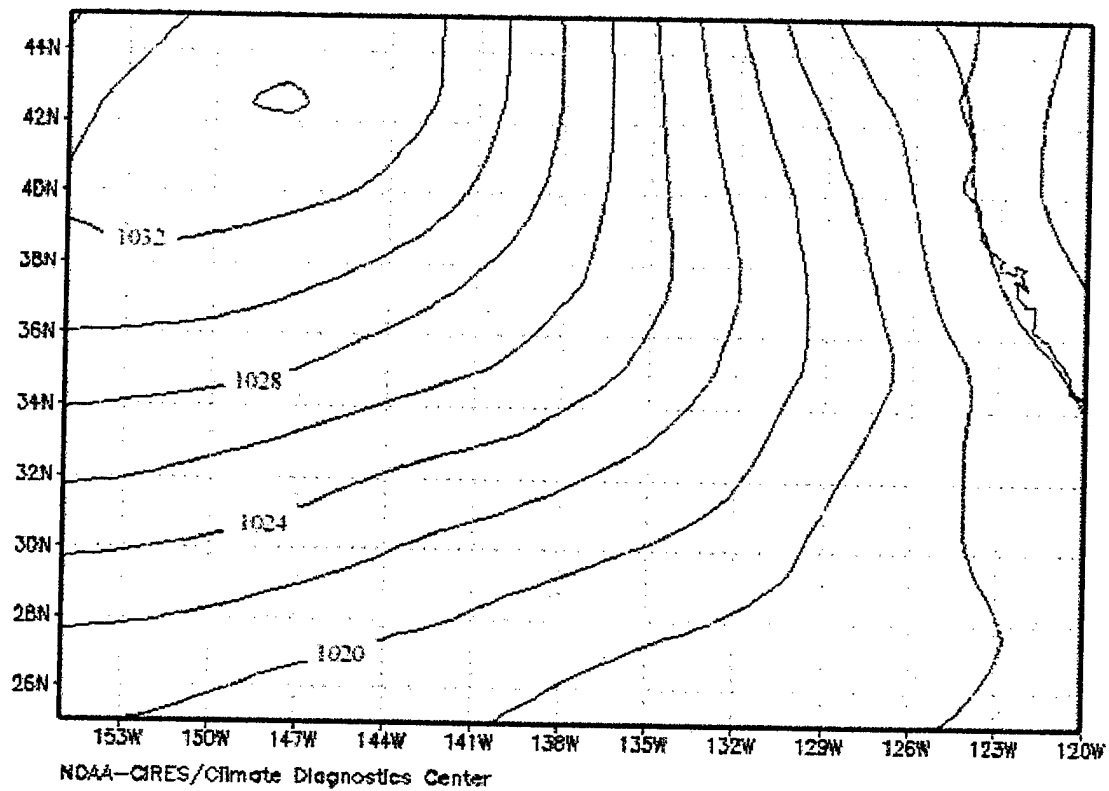


Figure 5. Surface Pressure Chart. July 16, 1999. A 1034 millibar high is located to the northwest with ridging to the southeast. From reanalysis of NCEP data.

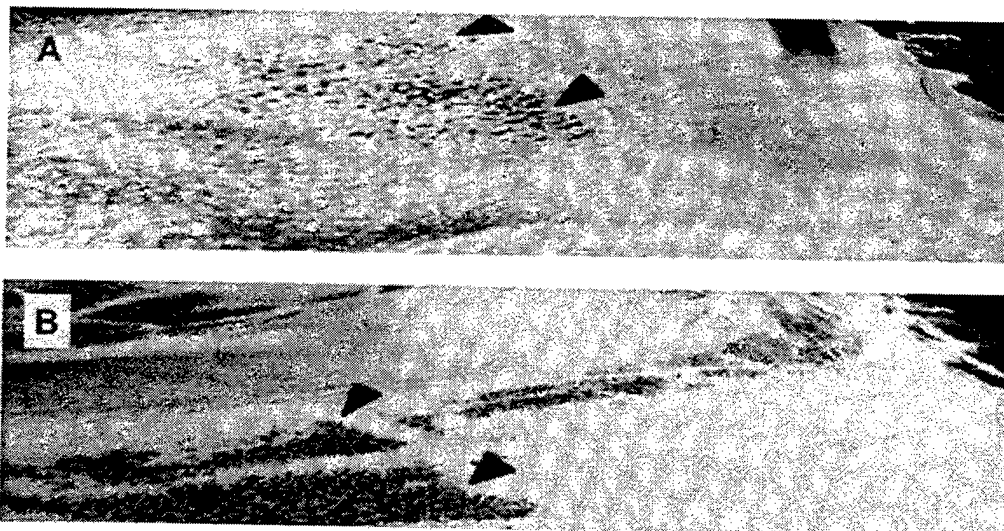


Figure 6. Evolution of the Cloud Rift. The overall rift complex extended 1400 kilometers west of the rift sampled by the CIRPAS Twin Otter. 6-A is an image taken at 0000 UTC on July 16, 1999. 6-B is an image taken at 1600 UTC the same day. The marked rectangular rift areas clear an area of 140,000 square kilometers.

B. ANALYSIS PROCEDURE

Measurement along the flight track provides a systematic look at the state of the atmosphere on both sides of the rift edge. A simple schematic of the flight tracks used in this study are shown in Figure 7. Table 1 provides a summary of the data investigated for this report. The CIRPAS aircraft collected data on four horizontal tracks across the rift boundary at flight levels of 30, 200, 400, and 630 meters. The flights at 30 and 630 meters are considerably valuable, showing the atmosphere at levels where significant gradients occur at the rift edge. Another lateral traverse of the rift while porpoising from an altitude of 600 to 800 meters reveals some interesting features of the clouds along the rift edge. Finally, two deep soundings, one within rift at station Tango, and one within the background cloud at Sierra, provide the vertical profiles of cloud bulk and microphysics properties as well as the boundary layer thermodynamic properties in the rift and in the background regions.

Direction	Altitude meters	UTC	Stations	Description
Horizontal Leg	30	1930	S → T	Low altitude transit
Horizontal Leg	200	2000	T → S	Marine boundary layer transit
Horizontal Leg	400	2100	T → S	Transit just below cloud bases
Horizontal Leg	630	2030	S → T	Transit 30 m below cloud tops
Porpoise	600 ⇌ 800	2130	S → T	Cloud tops transit
Vertical Leg	20 ⇌ 1200	1930	Sierra	Sounding of background cloud
Vertical Leg	20 ⇌ 1200	2000	Tango	Sounding of rift cloud

Table 1. Flight Path Summary

1. Background Clouds, Station Sierra

The original geographic position of Sierra was 260 kilometers west of Monterey Bay at 36°42'N 124°40'W. Solid cloud bases were observed at 400 meters and cloud tops were observed at 700 meters in the background cloudy region.

2. Rift clouds, Station Tango

The original geographic position of Tango was 36°08'N 124°15'W, approximately 100 kilometers south of Sierra. Cloud tops were observed at 650 meters. In the flight log (Haf Jonsson, personal communication), 'Ascent in clear air → descent through cloud to base: tops at [670 meters]. Nice stuff in the ultrafine – when entering the haze layer aloft both CN and Ultrafine concentrations collapse. A collapse in PCASP concentrations associated with a huge peak in the ultrafine at cloud top. Few, big drops in clouds.'

3. Cloud Rift Edge

The cloud rift edge was oriented east west at 36°10'N at 1830 UTC. The embedded rift feature and rift boundary advected southward through the time period. Notes taken from the flight logbook (Haf Jonsson, personal communication),

S → T: a shower encountered at 36°15'N.

As we approach the edge again [flight level: 685 meters], bimodal FSSP, few, big particles peak near channel 13. Edge at 36°10' – clean air, no counts in PCASP, but ultrafine jumps near the edge then goes away. Magnificently clean air!

Rift edge at 35°58'N again at cloud tops: CLEAN [free of optically active particles] + NEW [ultrafine] particles. Very dirty air above. It looks like the edge moved North big time—did we actually probe a disintegrating cloud deck?

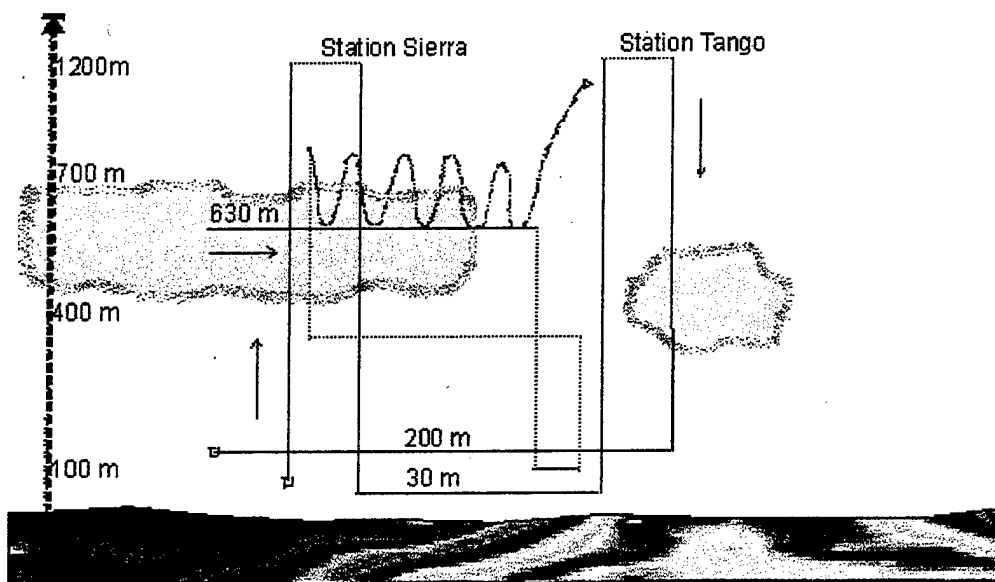


Figure 7. Flight Track Schematic. Four horizontal legs cross the rift boundary and two 1200 meter soundings mark the stations Sierra and Tango.

C. DATA AND ANALYSIS

The analysis focuses on environmental conditions at Sierra and Tango, and the rift edge -- a region of intense gradients between points Sierra and Tango. Data presented characterizes thermodynamic and microphysical properties observed at each location.

1. Description of the Background Cloud, Station Sierra

Figures 8-A and 8-C show vertical soundings at station Sierra and reveal a strong inversion capping the marine boundary layer. The temperature profile indicates a nearly dry adiabatic lapse rate to the base of the cloud deck and clearly defined inversion base at cloud top. Potential temperature is nearly constant up to the base of the clouds and shows a typical a step-like increase in potential temperature across the inversion. The dew point indicates a moist boundary layer and dry air aloft. Based on criteria described in Kuo and Schubert (1988), the jump in equivalent potential temperature and water mixing ratios across the base of the inversion indicate a stable stratocumulus cloud layer ($\Delta\theta_e \approx 2K > 0$).

Section A in the Appendix describes the process used to determine jump conditions across the inversion base.

Distinct cloud features are present in the liquid water concentration. Figure 9-A is the liquid water profile collected during the ascent and indicates a cloud base of 400 meters. The liquid water content increases linearly. Maximum liquid water content is measured at the cloud top; nearly 0.5 g m^{-3} .

Figure 10 shows the vertical profiles of the cloud droplet population in the background stratocumulus. The particle sensor data differs from the rift case with smooth, linear features apparent in cloud droplet effective radius (r_{eff}). Cloud droplet concentration (N_d) is nearly a constant within the cloud layer, a feature frequently observed in stratocumulus-topped boundary layer (Nicholls, 1984). Distinct boundaries are apparent near the cloud base and at the base of the inversion. Aerosol concentrations are shown in Figure 11-A and reveal a slight decline in counts descending below 100 meters. Aerosol measurements within the cloud were unusable. Aerosol counts are falsely registered when cloud droplets or drizzle splatter on the nozzle. The average concentration below cloud base is fairly constant at 700 cm^{-3} and rises to over 1000 cm^{-3} above the base of the inversion.

2. Description of the Rift Area, Station Tango

Figures 8-B and 8-D show vertical soundings at station Tango, and indicate a strong inversion is capping the marine boundary layer, but with notable differences. The potential temperature line is slightly tilted at the sea surface and a gradual increase potential temperature meets the base of the inversion. A step-like increase in potential temperature is not apparent. A gradual warming in potential temperature occurs below the

inversion and some cooling of the potential temperatures above it. Dew point temperatures match Sierra's up to 400 m. At this point the dew point falls off slightly, and dew points above the inversion show significant drying relative to station Sierra. The inversion strength remains strong, and applying the same stability criteria indicates a cloud-topped marine boundary layer at station Tango would be stable ($\Delta\theta_e \approx 3K$).

Despite available moisture and similar thermodynamic structure, clouds are scarce in the rift. Two liquid water profiles are presented in order to capture some of the variability associated with the rift feature. Liquid water traces shown in Figures 9-B and 9-C were taken during the ascent and descent, respectively. Variable cloudiness makes accurate sampling of rift clouds difficult, but the profiles reveals lower bases and cloud tops than in background clouds. Growth of the cloud droplets observed in the trace is erratic and broken, possibly due to the flight path of the sensor. Maximum liquid water content in the rift cloud is achieved at the cloud top, but clouds contain just 0.2 g m^{-3} .

The particle sensor data reveals a high degree of variability in the rift. Figure 10-B shows cloud droplet values in an ascent through virtually cloud free air with the exception of trace amounts of small droplets at 400 meters. A descent through broken clouds in the rift shown in Figure 10-C revealed large variations in cloud droplet r_{eff} for a given altitude and larger sizes than those observed in the background stratocumulus. Cloud droplet concentration drops by 25% from 80 to 60 cm^{-3} . Figures 11-B and 11-C show aerosol measurements in the rift. Figure 11-B is the cloud free case and shows a distinct reduction in effective particle sizes in a section of data where background stratocumulus was observed near station Sierra. Blocked out sections in Figure 11-B and 11-C are necessary

due to sensor contamination by drizzle or cloud droplets. The concentration of aerosols observed in the rift is about 1/6 that found in the layer below the background stratocumulus. Concentrations measured above the inversion remain approximately unchanged in relation to Sierra. Aerosol concentrations in the mixed boundary layer are clearly affected by the rift environment.

3. Description of the Rift Edge

Horizontal gradients observed at flight levels of 30, 200 and 630 meters reveal discontinuities at the transition from the background cloud to the cloud rift. In addition, a perturbation in the marine boundary layer height is evident in data collected while porpoising at the cloud top. The observations are plotted versus mission time in Figures 12-15 and illustrate horizontal gradients present at specific altitudes. The ground speed averaged 60 m/s for each horizontal leg so the 200 second tick marks represent about 10 km of horizontal distance traveled.

Figure 12 shows conditions observed near the air-ocean interface. The flight altitude was 30 m and the aircraft began under the background stratocumulus layer. Figures 12-A and 12-B represent total solar observed and aerosol concentration, respectively. Total solar irradiance is an excellent indicator of cloud cover above the aircraft. From the solar irradiance it appears that the aircraft emerges from background stratocumulus and into the rift between 9400 and 9600 seconds. The PCASP aerosol sensor records a significant drop coincident with the transition into the rift. Aerosol concentration is plotted in a logarithmic scale and indicates a slight increase in aerosol counts approaching the stratocumulus cloud edge of 100 cm^{-3} over a distance of 20 km. At

the cloud edge, aerosol counts fall nearly an order of magnitude and drop to just over 100 cm^{-3} .

Figure 13 shows total solar and aerosol distributions observed at 200 meters, and a similar drop in aerosol occurs at the rift boundary. The aircraft is within the rift at the start of the trace and enters background stratocumulus at approximately 12,000 seconds. The solar record indicates a few broken clouds are encountered before flying under the background stratocumulus. The observed difference in aerosol concentration across the rift edge is approximately 400 cm^{-3} . Noticeable scatter in aerosol concentration data is possibly due to spattering of drizzle drops on the sensor. Widespread drizzle in the 200 meter record verifies the likelihood of false counts. Again, a reduction in aerosol concentration is correlated to the rift edge.

Observations taken in a horizontal flight within the stratocumulus cloud shown in Figure 14 record a number of trends in cloud droplet size and concentration. The Twin Otter flew 30 meters below cloud tops at a flight level of 630 m and began in background stratocumulus. Figure 14-A is the solar trace and indicates the cloud edge is cleared at approximately 1020 seconds. Aerosol counts are not easily measured among the cloud droplets so the cloud droplet concentration is plotted in Figure 14-B. Figure 14-B shows increasing cloud droplet r_{eff} and decreasing N_d approaching the rift boundary. The cloud droplet effective radius increases from $14 \mu\text{m}$ at a distance of 15 km from the rift edge to $17 \mu\text{m}$ at the threshold. Cloud droplet concentration shows a proportionate decline from 40 cm^{-3} to slightly fewer than 30 cm^{-3} . Inside the rift, clouds exhibit droplet sizes ranging

from 12 to 18 microns. Clouds sampled in the rift contained fewer and larger cloud droplets than the background stratocumulus.

4. Rift Drizzle

Figure 15 shows distributions of drizzle measured using the CIP sensor. The plots show drizzle at the rift boundary and under broken clouds within the rift. The bands of drizzle are approximately 5 to 10 km across and coincide with the cloud features observed in Figures 12, 13 and 14. Drizzle appears to be most intense under the rift clouds (e.g. mission time 11,500 seconds to 11,700 seconds in Figure 15-A).

Drizzle appears to be an active element of the rift process. Drizzle was frequently detected inside the rift and at the rift edge, but not observed under background stratocumulus in this study. A rudimentary calculation using drizzle volume and cloud droplet sizes offers a conditional estimate of aerosol losses occurring in rift clouds due to drizzle. Figure 16 is a simple sketch of the basic elements of the conceptual model. The calculation assumes that each cloud droplet in the background stratocumulus contains one condensation nuclei and that drizzle droplets in the rift and at the rift edge are combinations of these smaller droplets containing multiple CCN particles. Under these conditions, and neglecting other aerosol sources and sinks, the loss of cloud droplets measured across the rift boundary should be equivalent to the number of droplets lost in collision and coalescence into drizzle drops at the rift edge and inside the rift.

The values used to assess the drizzle efficiency are representative values taken from data collected near the rift. Drizzle amount is calculated using observations taken in the horizontal flight at 30 m. These are the drops that are most likely to hit the surface and

remove CCN. The following relation is used to determine the theoretical loss of cloud droplets in a drizzling cloud.

$$\Delta N_d = N_D \left(\frac{R_D}{r_{eff}} \right)^3 \quad (4)$$

N_D and R_D are the drizzle concentration (cm^{-3}) and average size, respectively. Observed r_{eff} in background stratocumulus is the only other variable needed to estimate losses to collision and coalescence. The values used to calculate expected losses are listed in Table 2. Although variability is present in each parameter measured, losses can be estimated. Observed N_d in background stratocumulus averaged 50-60 droplets cm^{-3} and dropped to 28-35 at the rift edge. Droplet concentrations dropped even further in the rift to 12-20 cm^{-3} .³ Using r_{eff} in stratocumulus and the drizzle droplet parameters linked to each N_d deficit, equation 4 is solved for theoretical losses. Calculations indicate that drizzle accounts for the losses to N_d and captured CCN – compare ΔN_d theory and ΔN_d observed in Table 2.

	Stratocumulus	Edge	Rift Cloud	Description
N_d, cm^{-3}	50-60	28-35	12-20	Observed cloud droplets
N_D, cm^{-3}	0	0.09	0.15	Observed drizzle droplet
$r_{eff}, \mu\text{m}$	13.5	16	17	Cloud droplet effective radius
$R_D, \mu\text{m}$	0.0	75-85	80-100	Rain drop effective radius
$\Delta N_d, \text{theory}$	-	15-22	30-60	Lost cloud droplets
$\Delta N_d, \text{observed}$	-	24	40	Loss of cloud droplets, average

Table 2. Liquid Water Calculations

5. Cloud-topped Boundary Layer

The last set of flight data to be presented was gained by porpoising at cloud top from Sierra to Tango. The track is comprised of 10 soundings in and out of the tops of marine stratocumulus and rift cloudiness. The approximate locations are presented in Figure 17. Complex interactions between thermodynamics and microphysics occur at the rift boundary. The complete sounding series shows an upward slope to the cloud topped marine boundary layer approaching the rift and a dip in the MBL inside the rift. Three descents into cloud are shown in Figures 18 and 19. Sections taken at 3 locations do not provide the resolution to capture every detail in the transition, but offers a three dimensional view of changes. Figure 18-A shows temperature dew point profiles across the rift edge. Figure 18-B is a liquid water trace and shows the greatest LWC is in stratocumulus cloud near the rift edge. Clouds inside the rift contain less liquid water and lower cloud tops. Figure 19 shows cloud droplet population comparisons. N_d is fairly stable in the background clouds, averaging 50 to 60 cm^{-3} . Droplet sizes increase with height from 600 meters to the cloud top at 680 meters. Cloud droplets at the edge of background stratocumulus are larger at all levels within the cloud. N_d measurements here reveal higher concentrations near the cloud top. The rift section record shows the largest and fewest cloud droplets. The cloud top height drops to 650 m, similar to the drop recorded in the temperature profiles. This thin cloud feature averages 20 droplets cm^{-3} and r_{eff} is 17 μm at all levels within the cloud. Multiple transitions appear to be happening in this dynamic zone marking the edge of the rift.

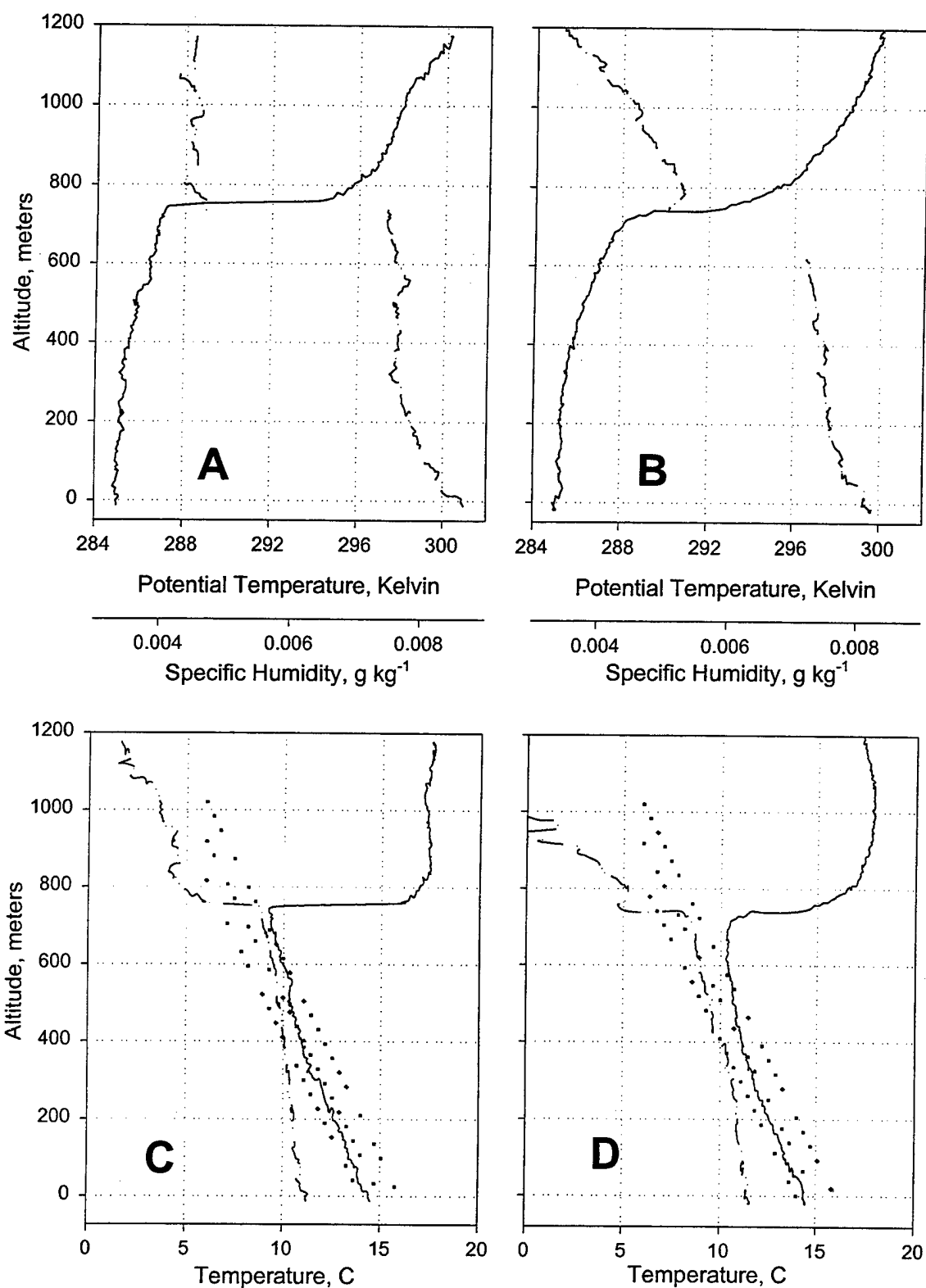


Figure 8. Boundary Layer Thermodynamics. 8-A and 8-C depict conditions observed at station Sierra. 8-B and 8-D are observations taken within rift at station Tango. Dotted lines in the lower figures represent the dry adiabatic lapse rate, Γ_d .

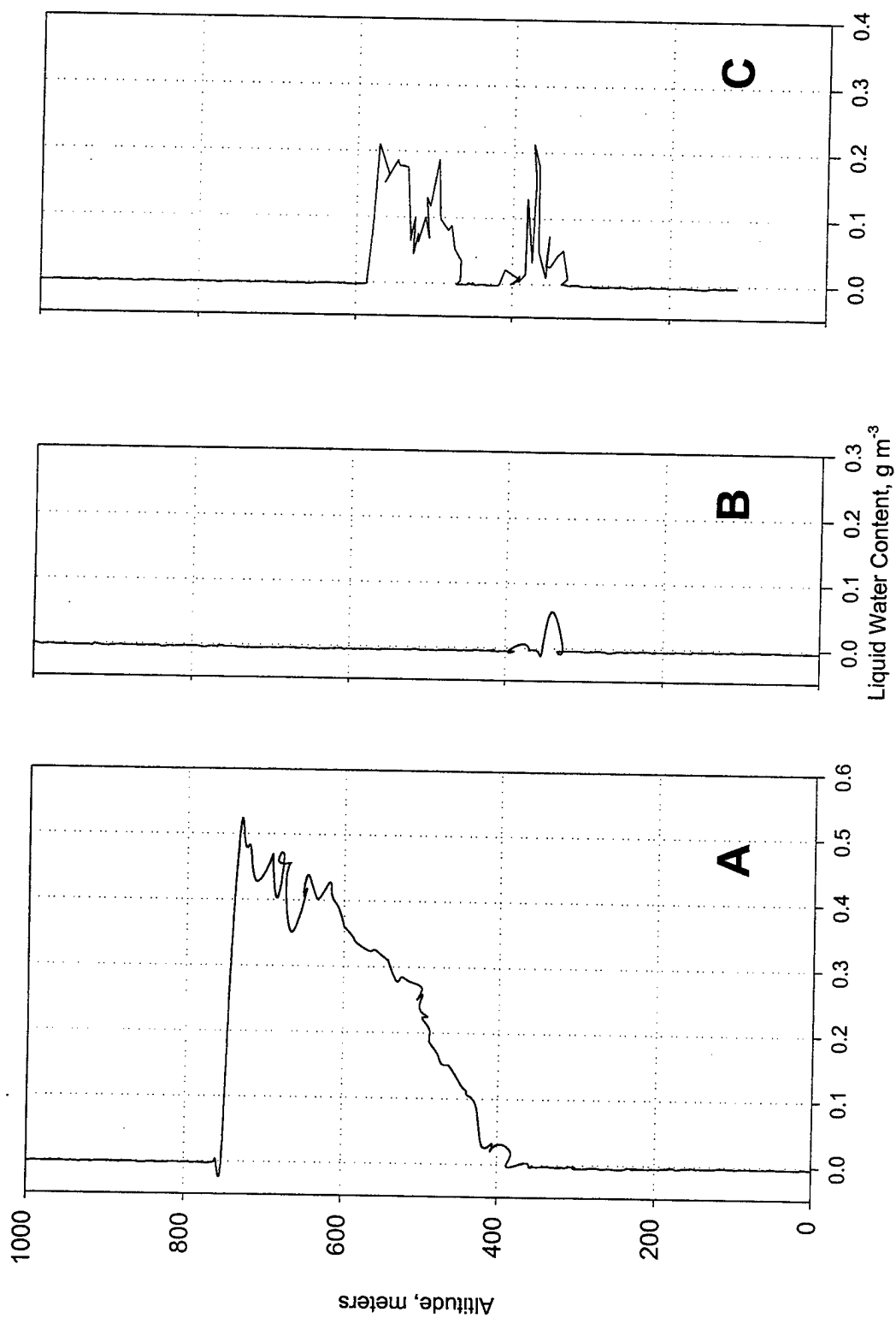


Figure 9. Liquid Water Concentration. 9-A is a liquid water trace taken at station Sierra, showing defined cloud tops and bases. 9-B is an ascent within the rift clear of clouds. Trace amounts of liquid water were observed. 9-C shows LWC in clouds observed inside the rift.

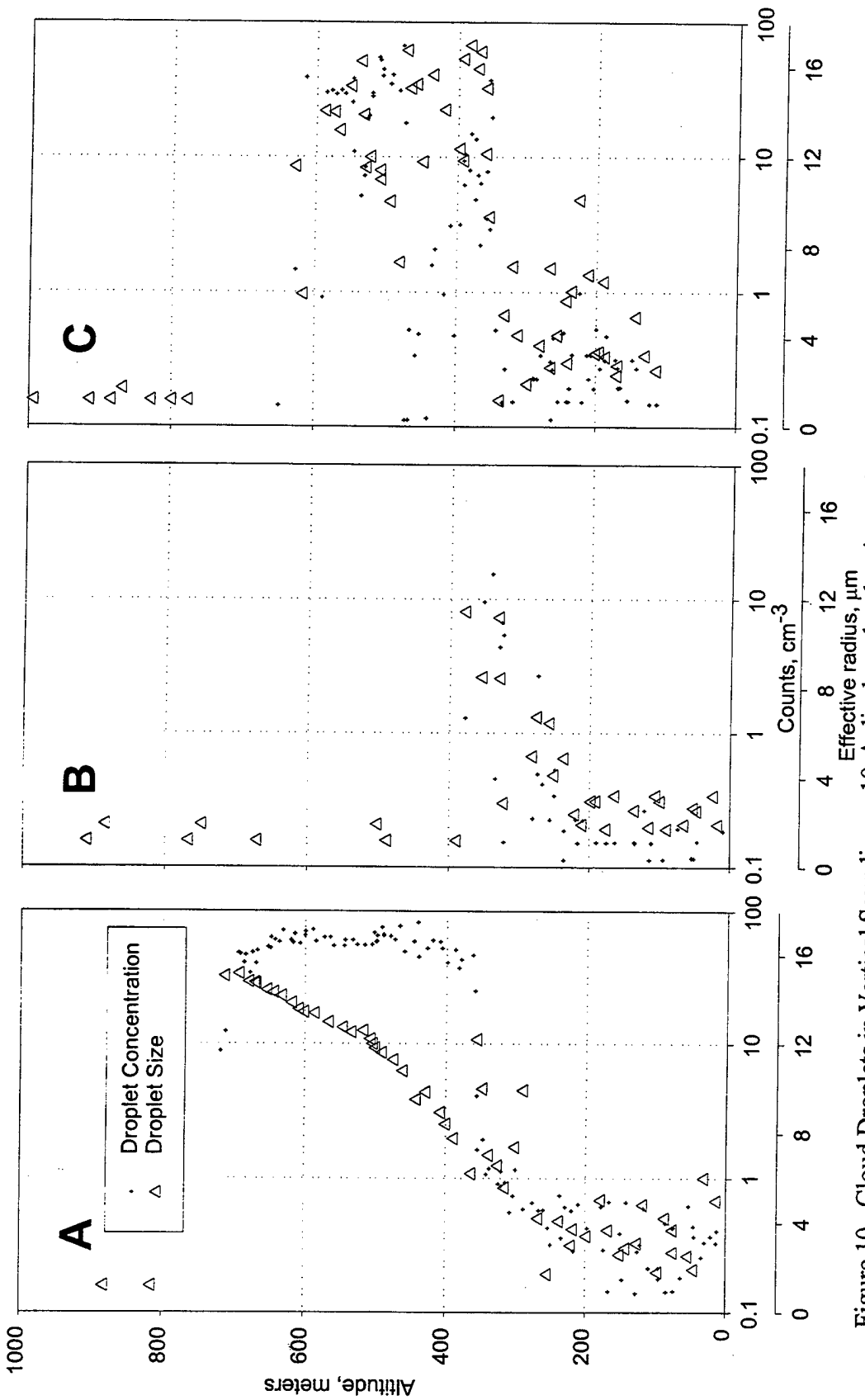


Figure 10. Cloud Droplets in Vertical Soundings. 10-A displays droplet size and concentration at station Sierra. 10-B was measured in a cloud free layer inside the rift. 10-C shows results from the descent through broken cloud elements inside the rift.

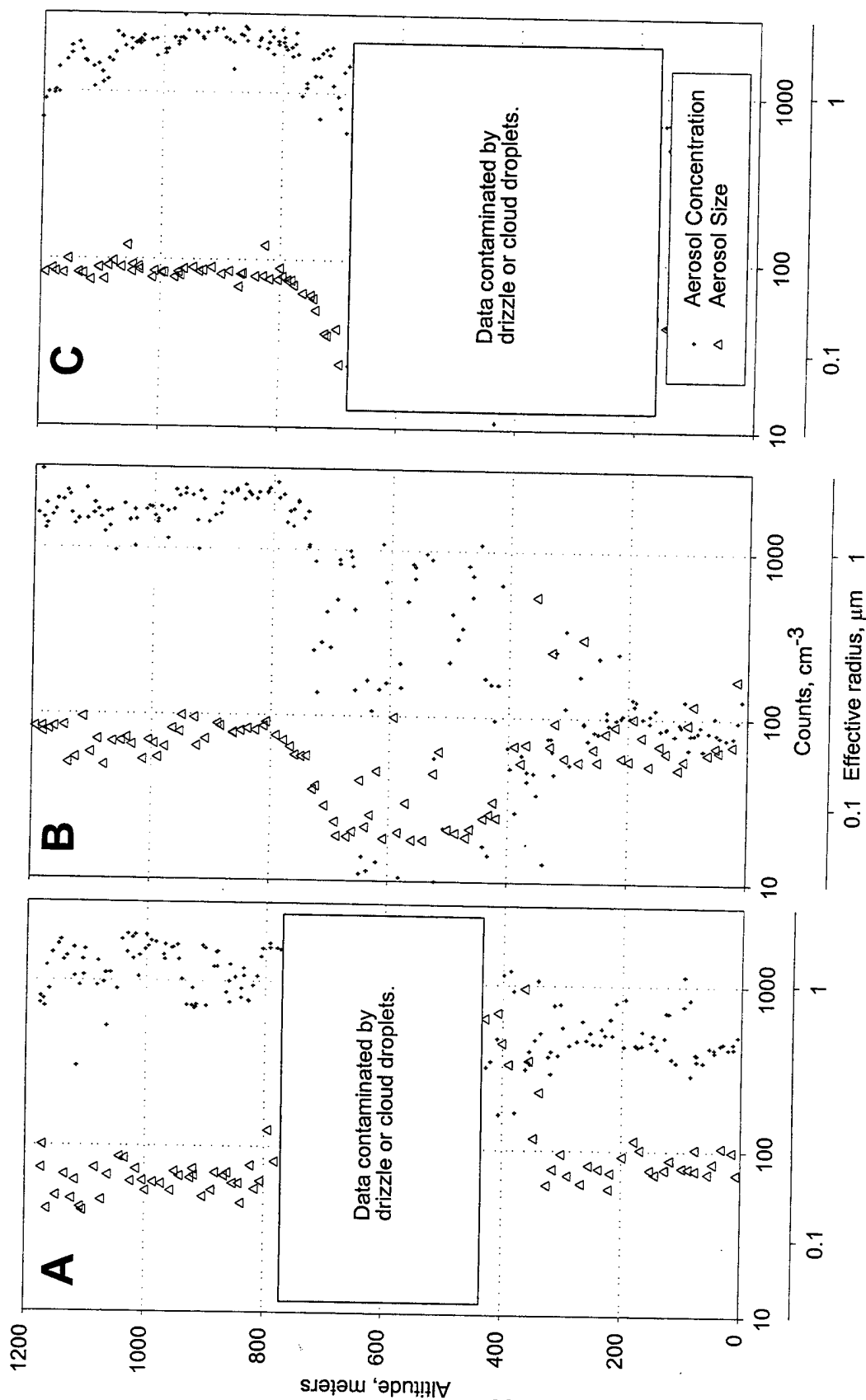


Figure 11. Aerosol in Vertical Soundings. 11-A displays aerosol size and concentration at station Sierra. 11-B is a nearly cloud free layer inside the rift. 11-C shows matches 11-B above the MBL but drizzle and cloud droplets contaminate the blocked data.

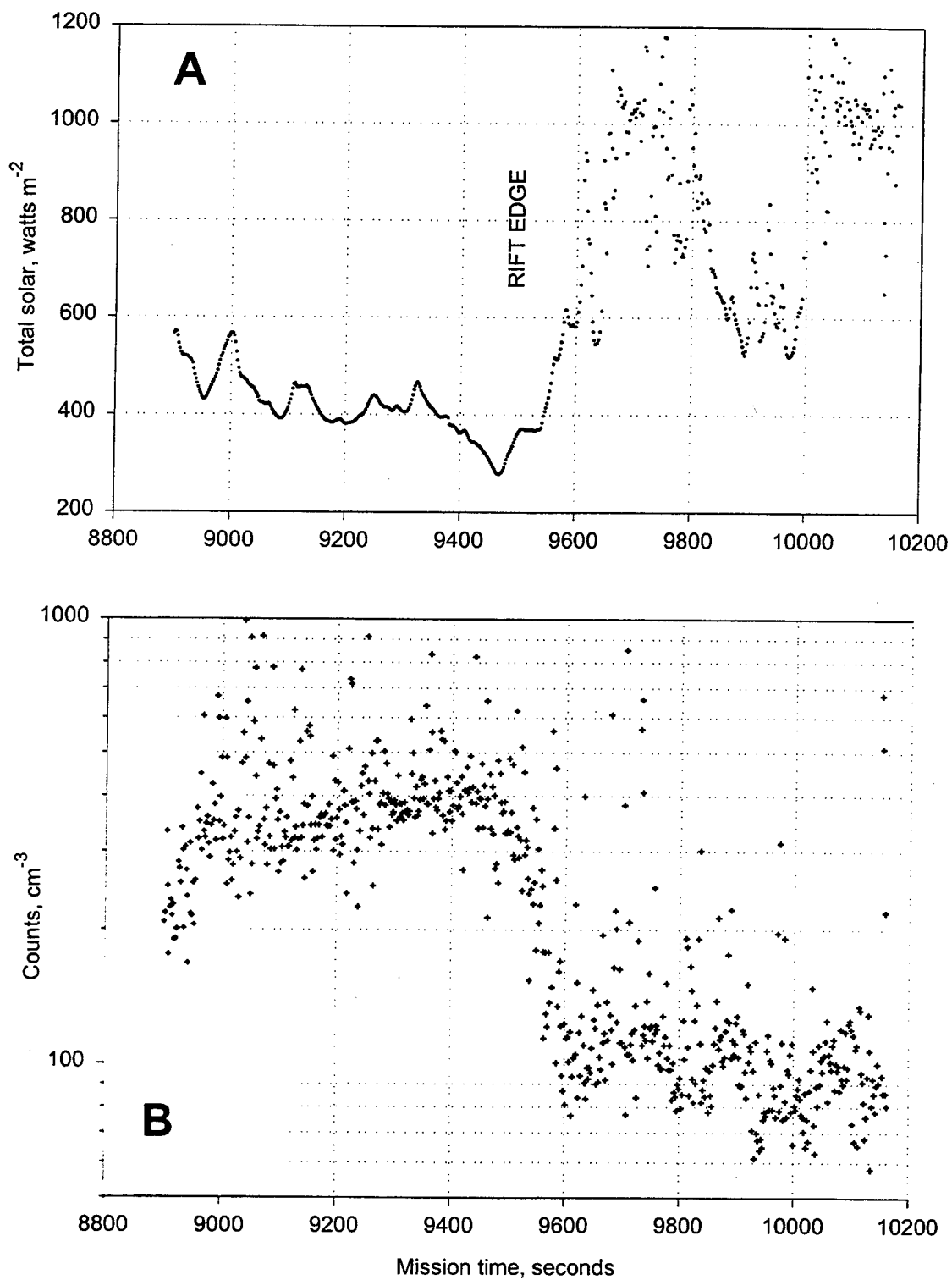


Figure 12. Rift Crossing at 30 m. 12-A and 12-B show total solar and aerosol concentration, respectively. The Twin Otter emerged from background clouds between 9400 and 9600 seconds.

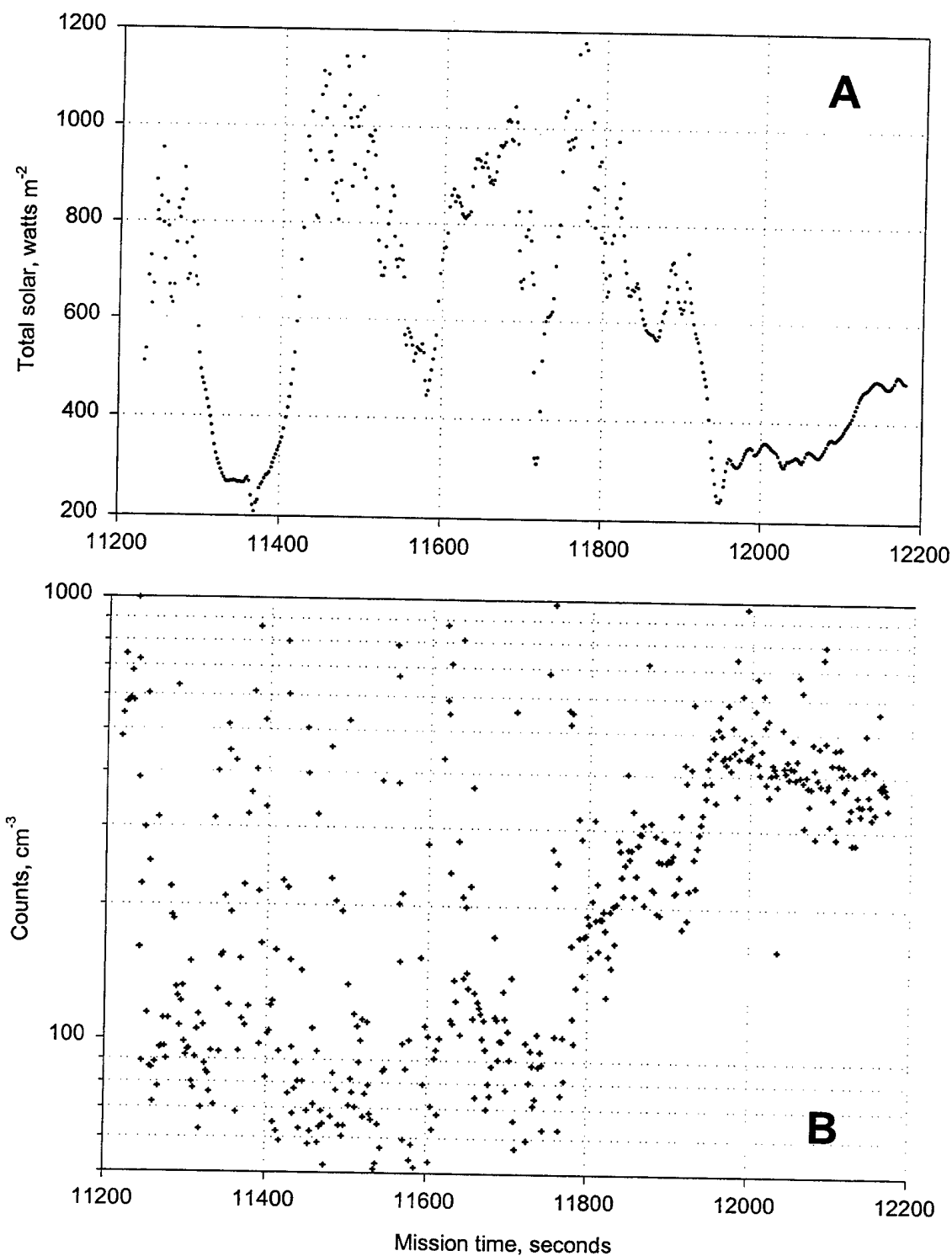


Figure 13. Rift Crossing at 200 m. Total solar and aerosol concentration are traced in 13-A and 13-B, respectively. The rift edge is crossed at approximately 12,000 seconds.

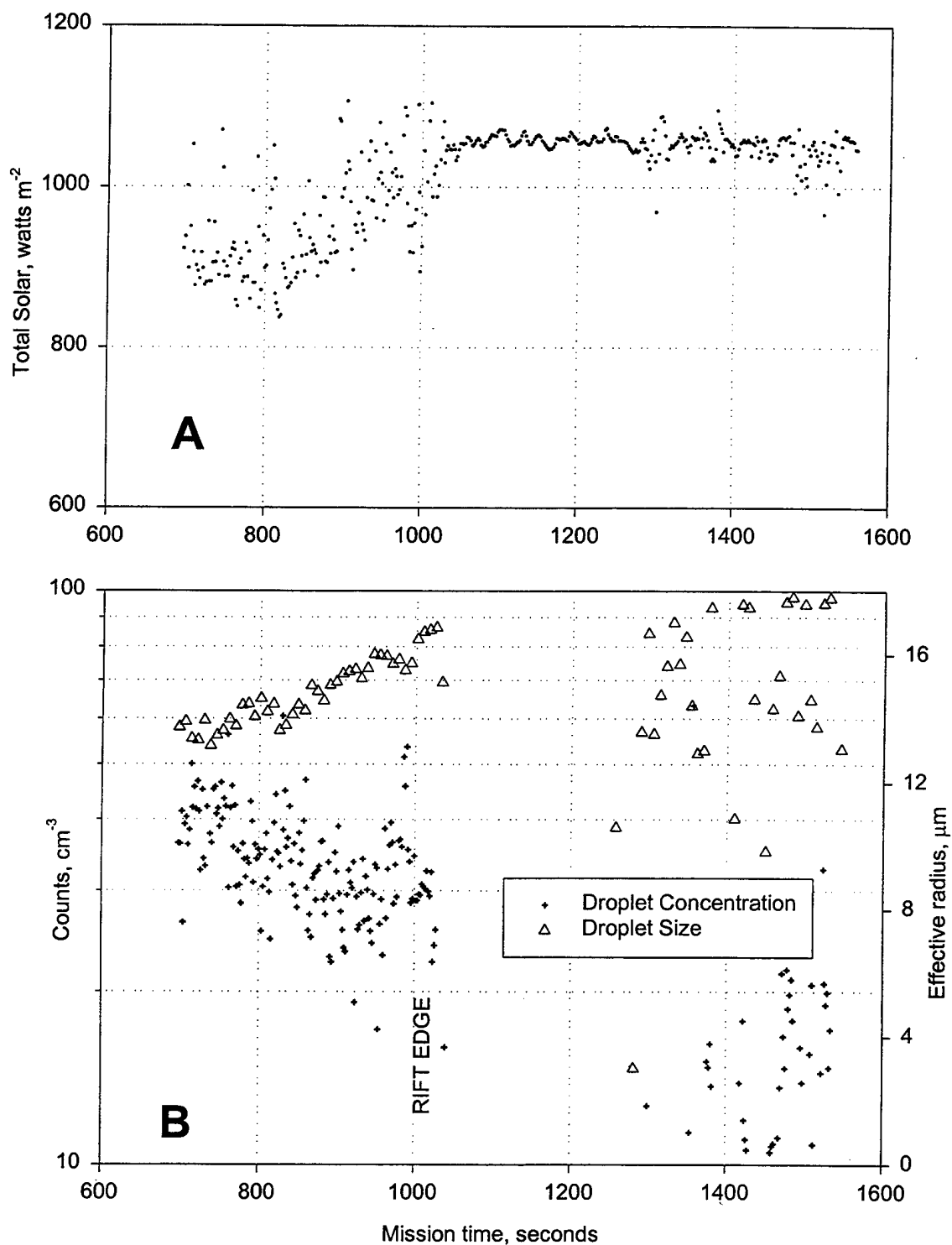


Figure 14. Rift Crossing at 630 m. Total solar indicates rift is reached at 1020 seconds. 14-B is measured cloud droplet size and concentration. Background stratocumulus is to the left of the rift edge marker.

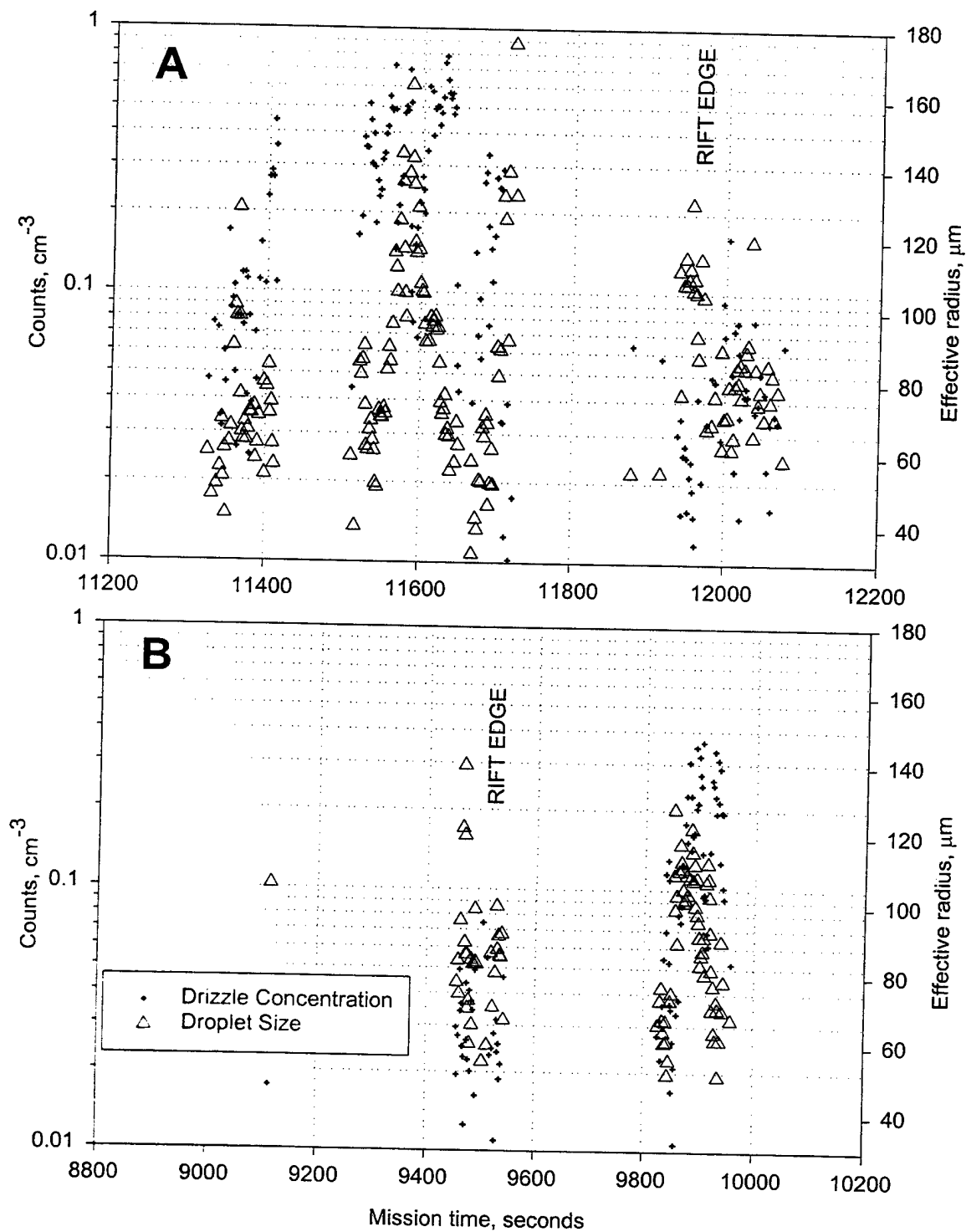


Figure 15. Drizzle Frequency. 15-A represents drizzle observed at 200 meters. The rift is located to the left of the rift edge marked in the 15-A. The rift is to the right of the rift edge marked in 15-B.

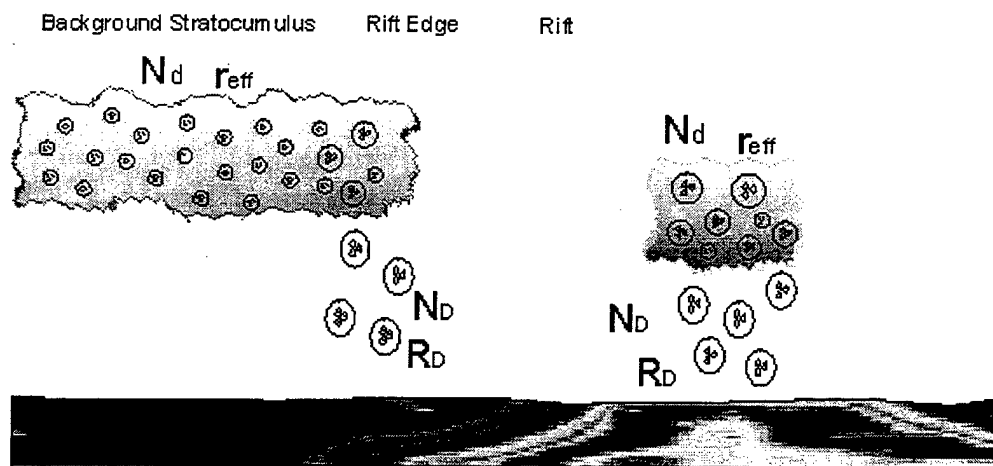


Figure 16. Drizzle Model. The loss of N_d observed across the rift edge is accounted for in a simple drizzle model. N_D and R_D are drizzle concentration and effective radius, respectively. N_d and r_{eff} are cloud droplet number and size.

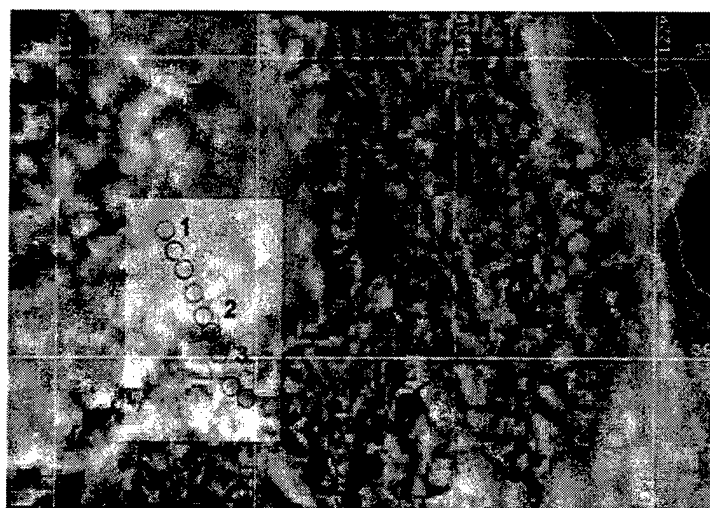


Figure 17. Cloud Top Flight Track. Circles indicate sites where the aircraft dropped in to measure cloud properties. Satellite image valid 2100 UTC.

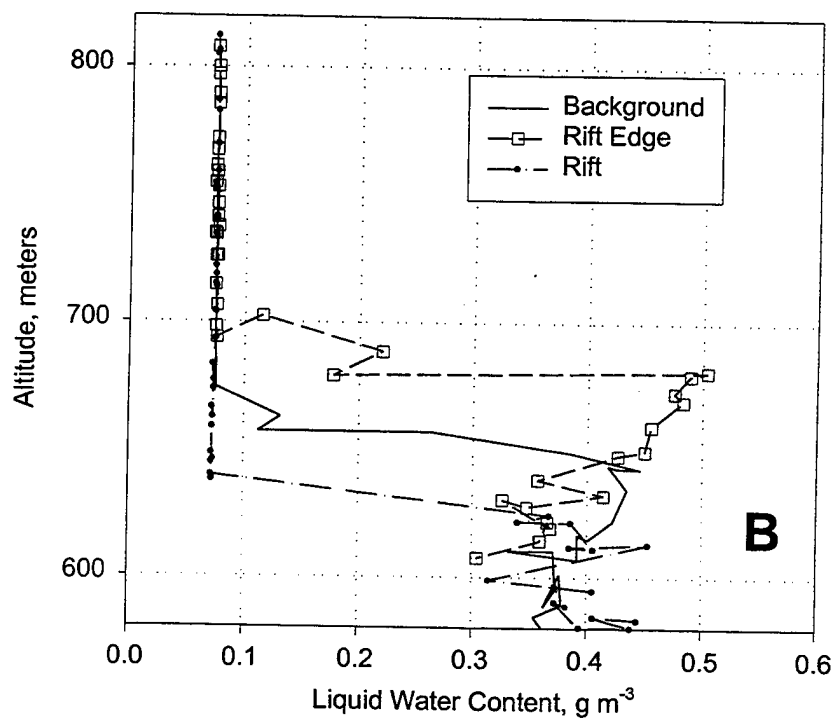
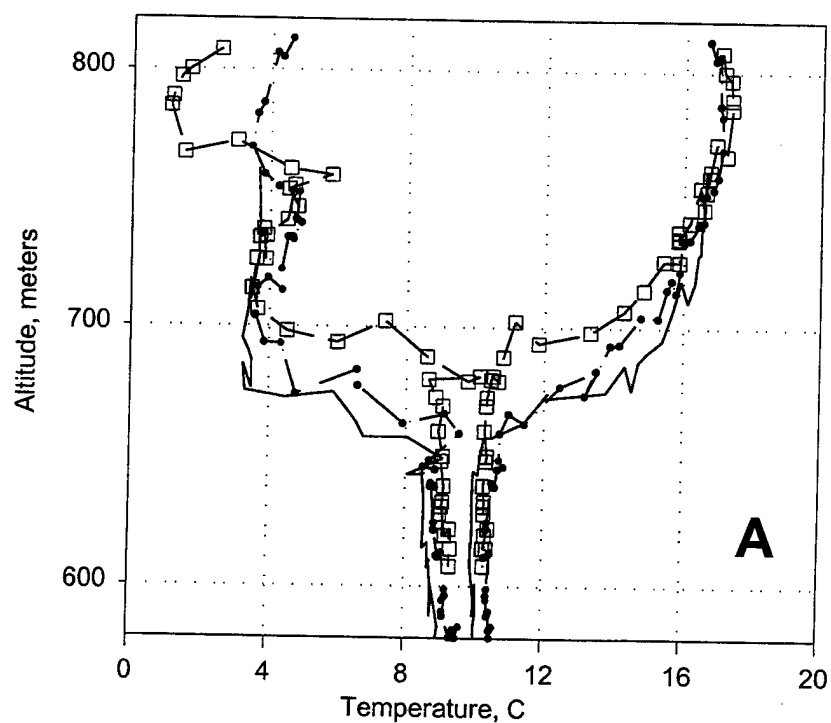


Figure 18. Rift Crossing at Cloud Tops. 18-A depicts temperature and dew point profiles near the cloud tops. 18-B shows the liquid water concentration profile at the same locations.

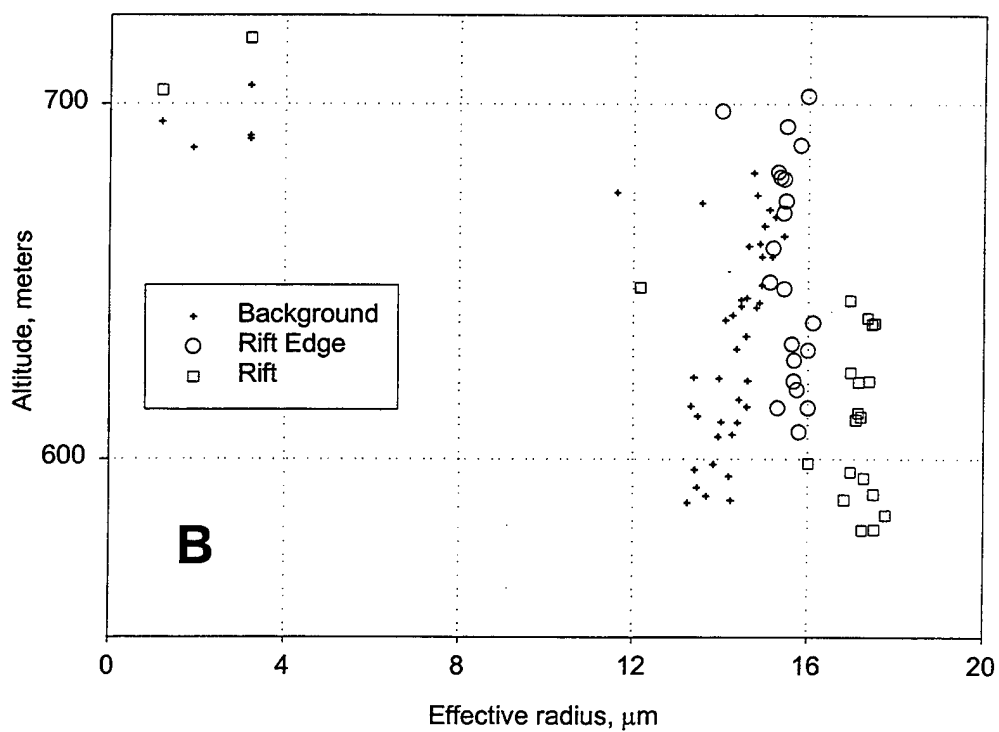
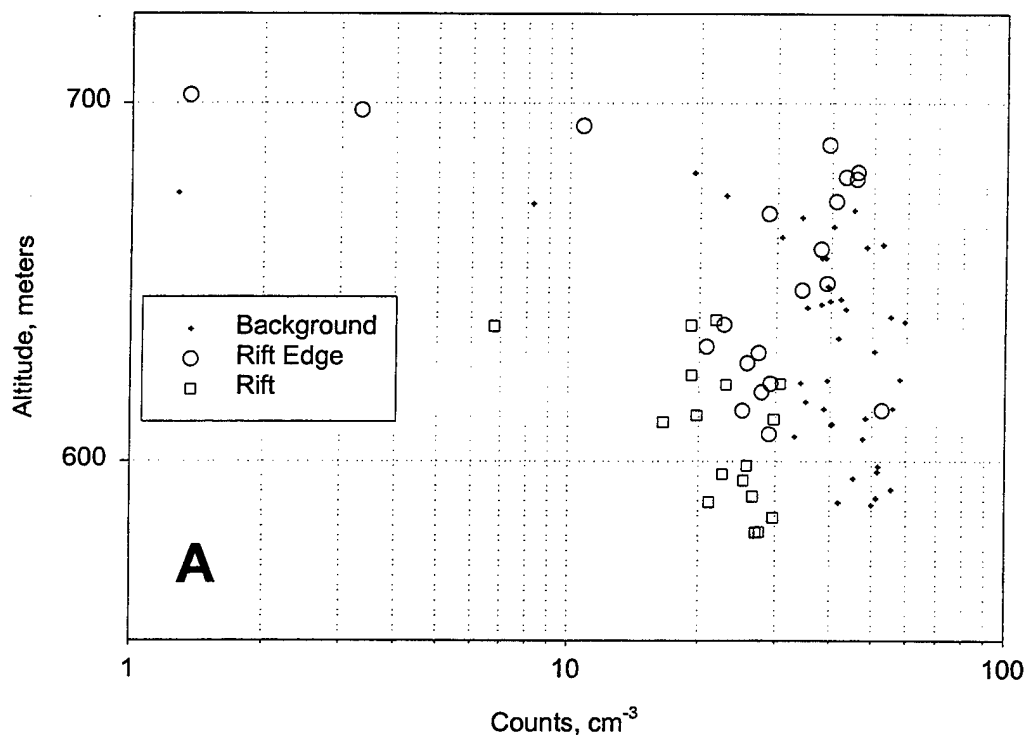


Figure 19. Rift Microphysics. 19-A plots cloud droplet concentration for locations shown in Figure 18. 19-B plots the droplet size distribution.

THIS PAGE INTENTIONALLY LEFT BLANK

IV. CONCLUSION

A. FINDINGS

The analysis presented in this study provides compelling evidence that rift formations are supported by scavenging of CCN by clouds and removal through the drizzle process. The satellite imagery and flight log provide the first indications of cloud collapse within a persistent background of marine stratocumulus. Thermodynamic profiles observed at stations Sierra and Tango reveal differences that are likely the result of the collapse of a persistent cloud layer acting on the inversion layer. The differences in cloud microphysics observed along flight tracks in stratocumulus and cloud rift indicate that cloud cover is correlated with aerosol concentrations. The depletion of aerosol is clearly confined to the rift area. Ambient cloud droplet populations exhibit droplet growth near the rift boundary, a precursor of collision and coalescence in marine clouds. Drizzle is observed at the cloud rift edge and under clouds in the rift, a manifestation of instability in the cloud droplet population. Drizzle is a CCN sink and the observed size and concentration of drizzle droplets are consistent with those necessary to account for the loss of aerosols observed across the rift. The analysis presented here supports drizzle as a trigger for rift formation and self-perpetuating cloud suppression mechanism.

B. RECOMMENDATIONS

The opportunity for additional research is clearly evident for this case study. Questions remain concerning how the drizzle process is initiated in particular regions. The data has been evaluated in a coarse fashion with minimal statistical review. Additional analysis of this data set should reveal more detail in the drizzle process. Several days of data are needed in order to completely describe the rift production sequence. Detailed analysis of meteorological conditions associated with the cloud rifts will reveal additional insight into to formation process. Finally, the overall significance of rifts will still remain unanswered until a long term survey of coastal marine stratocumulus is completed. A complete understanding of rift evolution and its frequency in marine stratocumulus may benefit other aspects of cloud research and may improve analysis of cloud radiative forcing.

LIST OF REFERENCES

- Ackerman, Andrew S., Owen B. Toon, and Peter V. Hobbs, 1993: Dissipation of marine stratiform clouds and collapse of the marine boundary layer due to the depletion of cloud condensation nuclei by clouds, *Science*, 262, 226-229.
- Albrecht, Bruce A., 1989: Aerosols, cloud microphysics, and fractional cloudiness, *Science*, 24, 1227-1230.
- Baker, M. B., 1997: Cloud microphysics and climate, *Science*, 276, 1072-1078.
- Durkee, P. A., K. J. Noone, and R. Bluth, 2000: The Monterey area ship track experiment, *J. Atmos. Sci.*, 57, 2523-2541.
- Hindman, E. E., W. M. Porch, J. G. Hudson, and P. A. Durkee, 1994: Ship-produced cloud lines of 13 July 1991, *Atmospheric Environment*, 28, 3393-3403.
- Hudson, J. G., and Paul R. Frisbie, 1991: Cloud condensation nuclei near marine stratus, *J. Geophys. Res.*, 96, 20,795-20,808.
- Ferek, R. J., T. G. Garret, P. V. Hobbs, S. R. Strader, D. Johnson, J. P. Taylor, K. Nielsen, A. S. Ackerman, Y. Kogan, Q. Liu, B. A. Albrecht, D. Babb, 2000: Drizzle suppression in ship tracks, *J. Atmos. Sci.*, 57, 2707-2728.
- Jonsson, H., 1999: Personal communication, CIRPAS Twin Otter flight log.
- Kuo, Hung-Chi., and Wayne H. Schubert, 1988: Stability of cloud-topped boundary layers, *Q. J. R. Meteorol. Soc.*, 114, 887-916.
- Nicholls, S., 1984: The dynamics of stratocumulus: aircraft observations and comparisons with a mixed layer model, *Q. J. R. Meteorol. Soc.*, 110, 783-820.
- Randall, D. A., 1980: Conditional instability of the first kind upside-down. *J. Atmos. Sci.*, 94, 292-309.
- Randall, D. A., J. A. Coakley, C. W. Fairall, R. A. Kropli, D. H. Lenschow, 1984: Outlook for research on subtropical marine stratiform clouds. *Bull. Am. Meteorol. Soc.*, 65, 1290-1301.
- Rogers, R. R., M. K. Yau, 1989: *A Short Course in Cloud Physics*, Third Ed. Butterworth-Heinemann, 290 pp.

Siems, S. T., C. S. Bretherton, M. B. Baker, S. Shy, and R. T. Breidenthal, 1990: Buoyancy reversal and cloudtop entrainment instability. *Q. J. R. Meteorol. Soc.*, 116, 705-739.

Twomey, S., M. Piepgrass, and T. L. Wolfe, 1984: An assessment of the impact of pollution on global cloud albedo, *Tellus*, 36, 356 – 366.

Warren, S. G., C. J. Hahn, J. London, R. M. Chervin, R. L. Jenne, 1988: *Global Distribution of Total Cloud Cover and Cloud Top Amounts Over the Ocean*, National Center for Atmospheric Research, Boulder, CO.

APPENDIX

A. DATA FILES AND FLIGHT TRACK

Mission data was organized using a variety of criteria. The first partition of data occurred during the collection. The flight record is broken at approximately 12,000 seconds. A computer crash in flight forced a reboot and restart in data collection. The two data sets are further divided by computers used onboard the CIRPAS aircraft to process data. Figures A-1 and A-2 depict the entire flight path of the Twin Otter. Table A-1 presents data gathered by aircraft sensors with the exception of the particle probes. The shaded boxes indicate parameters used in this study. Separate files contain the multi-spectral data collected by the particle sensors and are addressed in the next section.

Additional fields were derived from the sensor data. Potential temperature was derived using the standard definition. $\theta = T \left[\frac{1000}{P} \right]^k$. In this form T is in Kelvin and pressure(P) is in mb. Specific humidity(q) required a few steps. Vapor pressure(e) was obtained using the relative humidity values. $f \approx \frac{e}{e_s}$. Saturation vapor pressure was determined using $e_s(T) = 6.112 \exp\left(\frac{17.67T}{T + 243.5}\right)$, where e_s is in mb and T is in degrees C.

Now, with a calculated e and pressure values: $q = \varepsilon \frac{e}{p - (1 - \varepsilon)e}$. In evaluating the stability of the inversion layer, a tephigram was used to determine lifting condensation level temperature(T_c) in the equivalent potential temperature calculation:

$\theta_e = \theta \exp\left(\frac{2675w}{T_c}\right)$. In this calculation q was substituted for mixing ratio(w). A degree of uncertainty was introduced by these approximations but the stability calculations allowed for wide margins of error. A complete description of cloud top evaporative theory and the complete process used to determine jump operator values is given in Kuo and Schubert (1988).

COLUMN	File: GPS	NOANA	TUANA
1	Mission Time (s)	Mission time (s)	Mission time (s)
2	UTC	Temp (C)	Temp (C)
3	Lat (DDMM.mmm)	10Hz	10 Hz
4	Long (DDMM.mmm)	0.5Hz	0.5 Hz
5	Alt (m)		Az (acceleration in gs)
6	Lat (DD.ddddd)		Ay
7	Long (DD.ddddd)		Ax
8			Aerodyne H2O
9	Mission Time (s)		
10	GPS Week	UV (W/m**2)	Ps (mb)
11	GPS Time (s)	Total Solar (W/m**2)	Pt (mb)
12	Gmd Speed (m/s)	SST Tasco (V)	Pt-Ps (mb)
13	Gmd track (DDD.dd)	Partial Solar (W/m**2)	Atop-Abottom (mb)
14	Mission Time (s)	Gerber Re/10 (V)	Sstar-Sport (mb)
15		Gerber LWC (V)	
16	GPS Time (s)	Gerber PSA (V)	Irga CO2
17	Roll (DD.ddd)	Alt (2*V)	
18	Pitch (DD.ddd)	Dew Point (C)	Irga T
19	Heading (DDD.dd)	T Vaisala (C)	Irga H2O
20		RH Vaisala (%)	
21		T Rosemount (C)	T (C)
22		FT1	Lyman Alfa
23		FT1	
27		Rad Alt (ft)	TAS (m/s)
28		LWC (g/m^3)	Palt (ft)
29			ff (m/s)
30			ddd (deg)
31			Irga H2O (g/m^3)
32			Irga CO2 (mg/M^3)

Table A-1. Data Files.

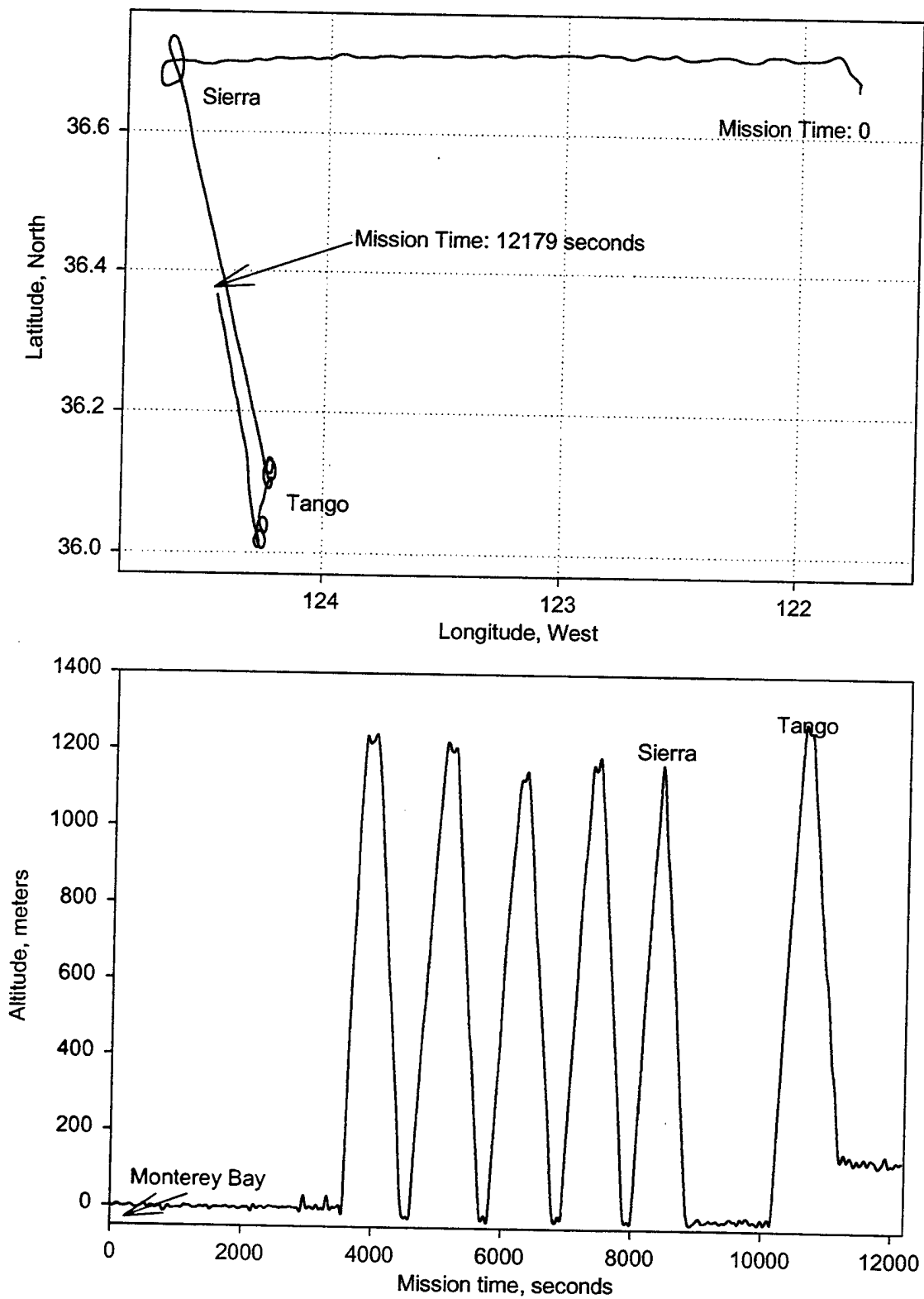


Figure A-1. Leg 1 Flight Track. The Twin Otter performed a sounding at Station Sierra and Tango in this record and two crossings of the rift boundary. The flight record lasts from 1800 UTC to 2000 UTC.

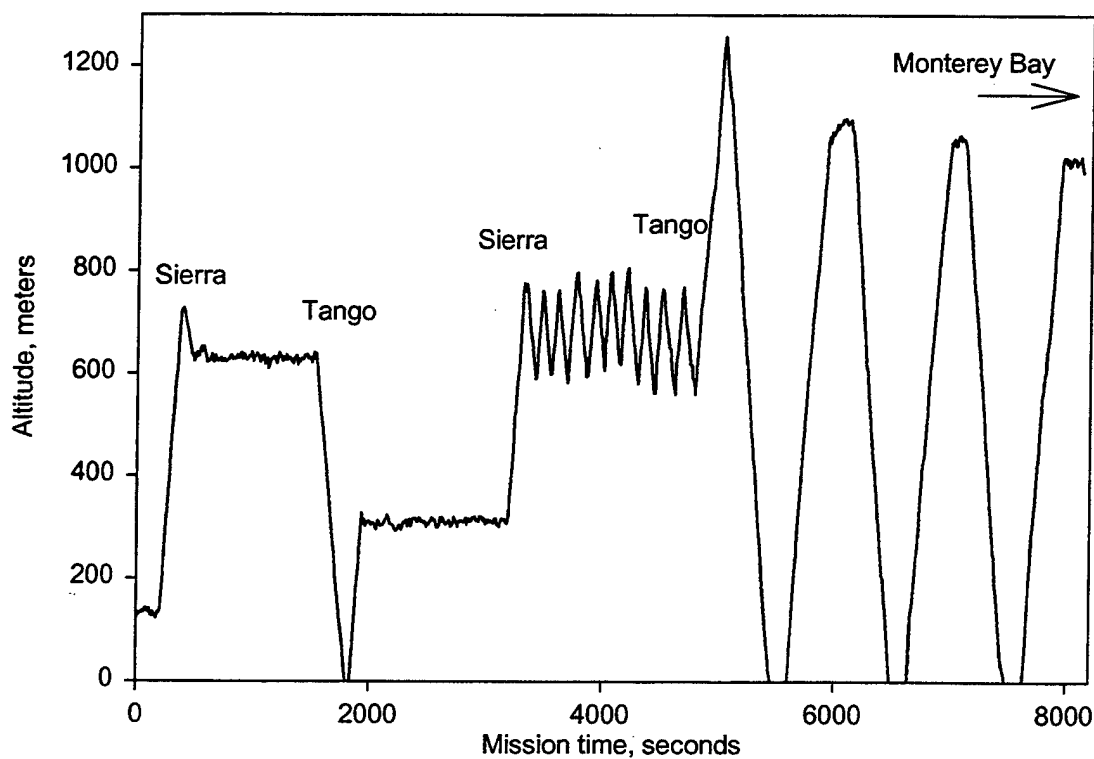
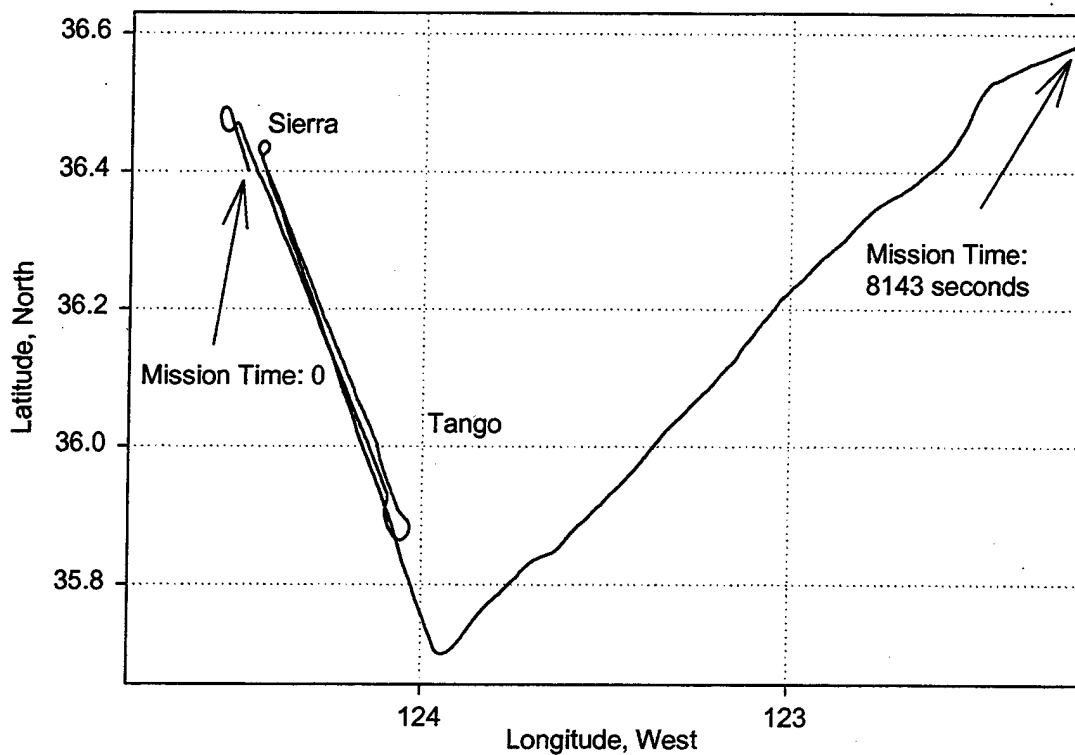


Figure A-2. Leg 2 Flight Track. The Twin Otter flew across the rift boundary three times in this record. The flight data was recorded between 2000 UTC and 2230 UTC.

B. PARTICLE PROBE DATA

The particle sensor data was originally analyzed in terms of particle diameters. Each sensor measured a spectrum of particles in 20-channel resolution. Channel information for the four sensors is listed in Table A-2. The three parameters given in Table A-2 specify channel lower limit, upper limit and geometric mean, respectively.

The sensor counts per channel indicate a concentration value normalized by the aircraft airspeed. The channel output values are given in terms of changes in counts(ΔN) observed in a cubic centimeter of sampled air. The summation of all channels for a given sensor provides a total count of particles in a given cubic centimeter(N_d). The effective radius calculation involved discretizing the integral form used with a continuous spectrum.

$$r_{eff} = \frac{\frac{4}{3} \int_0^{\infty} \pi r^3 n(r) dr}{\int_0^{\infty} \pi r^2 n(r) dr}$$

The term $n(r)$ is defined as $\frac{dN}{dr}$. In our discretized case $\Delta N \sim n(r)dr$. So, the equation relating measured values to a discrete effective radius becomes:

$$r_{eff} = \frac{\frac{4}{3} \sum_{i=1}^{20} \pi r_i^3 \Delta N_i}{\sum_{i=1}^{20} \pi r_i^2 \Delta N_i}$$

Incremental radius(r_i) and concentration (ΔN_i) values come directly from the particle probe data.

Sensor	PCASP (aerosol)			FSSP (droplets)		
	Diameter, microns			Diameter, microns		
Channel	Lower	Upper	G. Mean	Lower	Upper	G. Mean
1	0.10	0.11	0.10	1.50	2.10	1.77
2	0.11	0.13	0.12	2.10	3.90	2.86
3	0.13	0.14	0.13	3.90	5.90	4.80
4	0.14	0.15	0.14	5.90	7.70	6.74
5	0.15	0.17	0.16	7.70	9.90	8.73
6	0.17	0.20	0.18	9.90	11.60	10.72
7	0.20	0.24	0.22	11.60	13.50	12.51
8	0.24	0.27	0.25	13.50	15.00	14.23
9	0.27	0.29	0.28	15.00	17.50	16.20
10	0.29	0.32	0.30	17.50	19.00	18.23
11	0.32	0.36	0.34	19.00	20.00	19.49
12	0.36	0.73	0.51	20.00	21.00	20.49
13	0.73	0.96	0.84	21.00	21.60	21.30
14	0.96	1.30	1.12	21.60	22.60	22.09
15	1.30	1.45	1.37	22.60	23.30	22.95
16	1.45	1.63	1.54	23.30	24.50	23.89
17	1.63	1.84	1.73	24.50	25.60	25.04
18	1.84	2.10	1.97	25.60	27.00	26.29
19	2.10	3.00	2.51	27.00	28.30	27.64
20	3.00	4.00	3.46	28.30	30.40	29.33
	CAS			CIP (drizzle)		
	Diameter, microns			Diameter, microns		
Channel	Lower	Upper	G. Mean	Lower	Upper	G. Mean
1	0.40	0.60	0.49	15.79	39.58	25.00
2	0.60	0.75	0.67	39.58	63.16	50.00
3	0.75	0.83	0.79	63.16	89.06	75.00
4	0.83	0.88	0.85	89.06	112.28	100.00
5	0.88	0.96	0.92	112.28	139.16	125.00
6	0.96	1.10	1.03	139.16	161.69	150.00
7	1.10	1.30	1.20	161.69	189.41	175.00
8	1.30	2.90	1.94	189.41	211.19	200.00
9	2.90	4.80	3.73	211.19	239.72	225.00
10	4.80	6.20	5.46	239.72	260.72	250.00
11	6.20	7.70	6.91	260.72	290.06	275.00
12	7.70	10.00	8.77	290.06	310.28	300.00
13	10.00	12.30	11.09	310.28	340.41	325.00
14	12.30	34.00	20.45	340.41	359.85	350.00
15	34.00	39.00	36.41	359.85	390.78	375.00
16	39.00	45.00	41.89	390.78	409.43	400.00
17	45.00	45.00	45.00	409.43	441.16	425.00
18	45.00	45.00	45.00	441.16	459.02	450.00
19	45.00	45.00	45.00	459.02	491.54	475.00
20	45.00	45.00	45.00	491.54	508.61	500.00

Table A-2. Particle Sensor Channels.

THIS PAGE INTENTIONALLY LEFT BLANK

INITIAL DISTRIBUTION LIST

1. Defense Technical Information Center2
 8725 John J. Kingman Road, Suite 0944
 Ft. Belvoir, VA 22060-6218

2. Dudley Knox Library2
 Naval Postgraduate School
 411 Dyer Road
 Monterey, CA 93943-5101

3. Roddy Rogers1
 National Science Foundation
 4201 Wilson Boulevard, Room 775 S
 Arlington, VA 22230

4. Haf Jonsson1
 CIRPAS
 3240 Imjin Road, Hanger 510
 Marina, CA 93933

5. Philip Durkee2
 Department of Meteorology
 589 Dyer Road, Room 254
 Monterey, CA 93943-5114

6. Qing Wang1
 Department of Meteorology
 589 Dyer Road, Room 254
 Monterey, CA 93943-5114